GEOPHYSICAL INSTITUTE

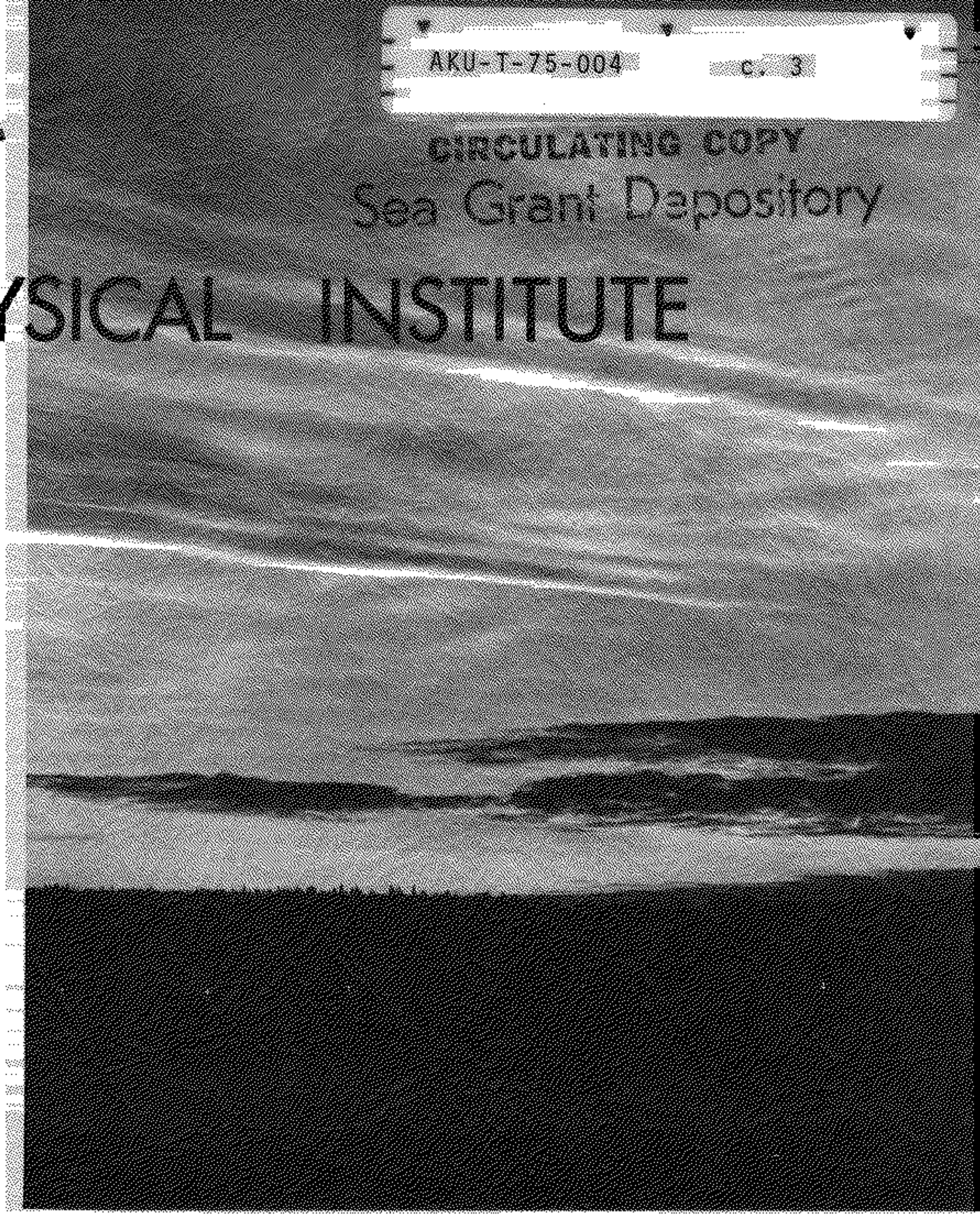

UNIVERSITY
OF ALASKA

FAIRBANKS,
ALASKA

UAG R-237

NEARSHORE PERMAFROST STUDIES IN THE VICINITY OF POINT BARROW, ALASKA

by

James C. Rogers
William D. Harrison
Lewis H. Shapiro
Thomas E. Osterkamp
Larry D. Gedney
J. Douglas VanWormer

SCIENTIFIC REPORT

May 1975

Sea Grant Report No. 75-6

NEARSHORE PERMAFROST STUDIES

IN THE VICINITY OF POINT BARROW, ALASKA

James C. Rogers
William D. Harrison
Lewis H. Shapiro
Thomas E. Osterkamp
Larry D. Gedney
J. Douglas VanWormer

Geophysical Institute
University of Alaska
Fairbanks, Alaska 99701

May 1975

Geophysical Institute Report No. UAG R-237
Alaska Sea Grant No. 75-6

TABLE OF CONTENTS

LIST OF FIGURES

LIST OF FIGURES (cont'd)

LIST OF ILLUSTRATIONS

LIST OF TABLES

ABSTRACT

Two principal areas of investigation were pursued during 1974. The first consisted of seismic refraction studies at Pt. Barrow, Alaska, and on Tapkaluk Island. The second involved laboratory analysis of soil sample thin sections and a theoretical analysis of permafrost response to an ocean transgression.

All seismic velocities measured in consolidated materials were found to fall into two groups. Velocities ranging from 1500 m sec^{-1} to 2000 m sec^{-1} were characteristic of the non-ice bonded sandy gravels while velocities from 2500 m sec^{-1} to 3000 m sec^{-1} were typical of that material when ice-bonded. A continuous high velocity refractor was observed along Barrow Spit at a depth of 1 meter and confirmed to be bonded permafrost. However, this refractor was not observed beneath Elson Lagoon immediately adjacent to Barrow Spit. From the refraction data, it is concluded that continuous ice-bonded permafrost does not exist in the northwest end of Elson Lagoon to depths of at least 150 m. Investigation of the spit between Plover Point and Point Barrow revealed no bonded permafrost to at least 47 m, while work on Tapkaluk Island, site of drilling investigations by others, indicated no continuous ice-bonded permafrost to depths of at least 50 m.

Near-surface cores from Barrow were taken and used in the development of a thin-sectioning technique for structural studies of frozen ground. Thermal conductivity apparatus was constructed and a theoretical analysis of the thawing of ice-bonded permafrost after a transgression of the ocean was carried out. In a simple model solved in

closed form, the thawing rate is little affected by the thermal properties or ice content of the material, but is controlled primarily by the rate of diffusion of salt. This illustrates the importance of mass transport and chemical processes in determining the off-shore permafrost regime.

INTRODUCTION

The discovery of oil reserves along the Arctic coast has focused increased attention on the interaction between permafrost and man's activities there. Of particular concern is a knowledge of the distribution and character of this permafrost both along the Arctic slope region and in the coastal zone as well as along the barrier islands and beneath the bottom of the Arctic Ocean. It is the purpose of this report to discuss permafrost distribution along the coast and offshore in the vicinity of Pt. Barrow. This discussion includes the presentation of some seismic results obtained by the University of Alaska in the fall of 1974. Ongoing theoretical and experimental studies of soil thermal and chemical properties in the near-shore region are also discussed. It is anticipated that results, such as those presented, will be useful for designing engineering structures such as harbor facilities, offshore drilling platforms, and submarine oil pipelines.

The work discussed in this report represents part of the efforts of the University of Alaska Sea Grant Program, and although the principal funding for the project was through the University of Alaska Sea Grant Office, several other agencies and organizations supported the work financially or logistically. This support is detailed and acknowledged later.

SECTION A

SEISMIC INVESTIGATION OF THE COASTAL PERMAFROST DISTRIBUTION AT PT. BARROW

I. OVERVIEW

This section of the report, which deals with seismic investigation of near-shore permafrost, describes the field work and the results obtained during the 1974 field season. A general discussion of permafrost distribution is followed by details of the seismic refraction method used and a description of the field work and data reduction method. Finally, results and conclusions are presented. The appendices contain particulars on the refraction method as well as time-distance plots for all the refraction lines run.

II. PERMAFROST DISTRIBUTION ALONG THE ARCTIC COAST OF ALASKA

Published permafrost maps of Alaska are quite general and are small in scale (Ferrians, 1965); however, one conclusion can be immediately made with respect to northern Alaska: Although there are several major zones of the permafrost regions, the area north of the Brooks Range is generally underlain by thick permafrost. Of the five recognized factors that control and affect the distribution of permafrost -- climatic, geologic, hydrologic, topographic and biologic -- climate is the principal factor that determines the regional distribution (Ferrians and Hobson, 1974). The mean annual temperature at Barrow and Prudhoe Bay is about -12°C (Johnson and Hartman, 1969), but the permafrost thickness at Prudhoe Bay is about 610 m, a figure approximately twice that at Barrow. Ferrians and Hobson (1974) attribute the difference in thickness to the difference of the thermal conductivity of the sediments and the corresponding decrease in the geothermal gradient at Prudhoe Bay with respect to Barrow.

In addition to the permafrost found under the land along the Beaufort Sea coast, permafrost has been reported beneath the ocean near the mouth of the MacKenzie River (Hunter and Hobson, 1974). There are two principal reasons to suspect the presence of permafrost beneath the Arctic Ocean along the coast. First, the level of the Arctic Ocean has varied considerably in the last 50,000 years. These variations are represented by a series of marine transgressions and regressions (Sellman and Brown, 1974). Thus, it is known that soil which was once above water and subject to permafrost formation due to the low temperatures is now covered by the ocean. Lachenbruch (1957) calculates that a rapidly transgressing shore line in the Barrow area would preserve permafrost in the ocean bottom. His calculations indicate possible permafrost to depths of about 60 meters at distances of one kilometer from shore. The second factor suggesting the existence of bottom permafrost is the ocean bottom temperature. Typically, this is on the order of -1.0°C (Lewellen, 1974). Therefore, any relict permafrost beneath the ocean would be preserved. Of course, the thickness would not be so great as for the original (above the water) situation where the surface temperature was perhaps -12°C.

Recently, Lewellen (1974) reported a series of temperature measurements near Barrow that show the average temperatures below Elson Lagoon and the barrier islands to be less than 0°C. Temperatures at depths of 2 to 4 meters below the bottom were about -1 to -1.5°C and showed little variation from summer to winter. Thus, these bottom materials fit the classic definition of permafrost: "Material that normally stays at or colder than 0°C over two years."

III. SEISMIC DETECTION OF PERMAFROST

The most direct method of permafrost detection is simply to drill a hole into the material of interest, measure the temperature *in situ* and examine cores recovered for water and ice content. However, this is expensive, and it is desirable to use methods which will provide information on the distribution of permafrost over a large area. Using the fact that seismic waves travel faster in frozen soils containing water than in non-frozen soils, it is possible to use standard seismic refraction techniques to detect bonded permafrost, both on land and beneath the ocean (Hunter, 1974). Appendix I contains a brief review of the seismic refraction technique and an estimate of the minimum penetration depth of seismic energy. Figure 1 is a compilation of laboratory and field measurements for frozen materials (Hunter, 1974). The lack of a one-to-one match between velocity in frozen material and material type requires that, in any field situation, ground truth be established by drilling.

It should be pointed out that the seismic refraction technique is useful for detecting some frozen materials, but not all permafrost covered by the definition given earlier can be detected using the technique. For example, solid rock at +1°C and at -1°C shows no significant velocity difference. Also, materials with large amounts of salt brine inclusions may not be frozen at -1°C and thus would not exhibit the

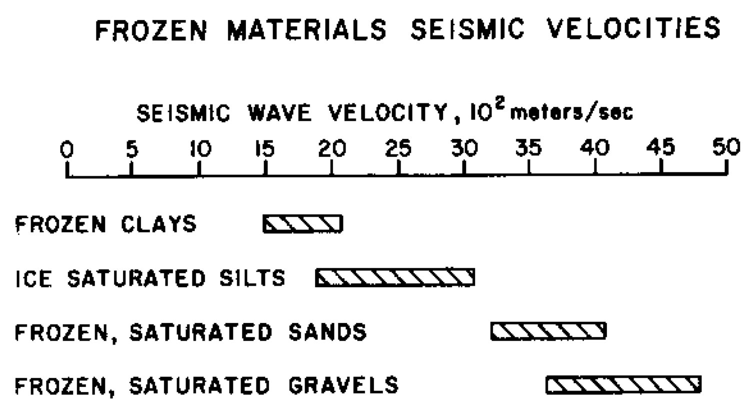

Figure 1. Seismic velocity measurement in frozen materials (from Hunter, 1974). Note that the values are only approximate and that velocity depends upon temperature, the porosity of the material and the degree of water saturation.

higher velocities associated with the freezing of interstitial water. However, for engineering purposes, while it is useful to know whether material is permafrost according to the above definition, it is more important to know whether the material is bonded. Thus, it is important to know whether the ocean sub-bottom material is bonded for the purposes of excavating and emplacement of hot oil pipelines. In such cases, the seismic technique proves useful. Of course the designer must have additional information such as moisture content to determine whether subsidence is a possible result of emplacing a hot oil pipeline in the bonded material. The seismic investigation discussed later in this report was not sophisticated enough to determine such factors as moisture content or material grain size, although there may be seismic methods of determining this information (McGinnis et al., 1974; Palowictz, 1971; Rothelisberger, 1972; Bell et al., 1973).

Another feature of seismic refraction work that is of importance to these investigations is the averaging nature of the technique. The simple geometry seen in Figure 2 indicates that the difference in travel time from the source to points 5, 6 or 7 is directly related to the distance between points 5, 6 and 7. However, if layer 2 is a relatively homogeneous material containing inclusions of massive ice it is possible that the seismic data will contain apparent anomalies. Whether such effects are seen in the data depends, among other factors, upon the velocity differences between the ice inclusion and the surrounding material, the relative size of the inclusion compared to the shot point spacing, and the time resolution of the seismic equipment. Dobrin (1960) discusses techniques for mapping large inclusions in otherwise

TWO LAYER EARTH: SEISMIC ENERGY PATHS

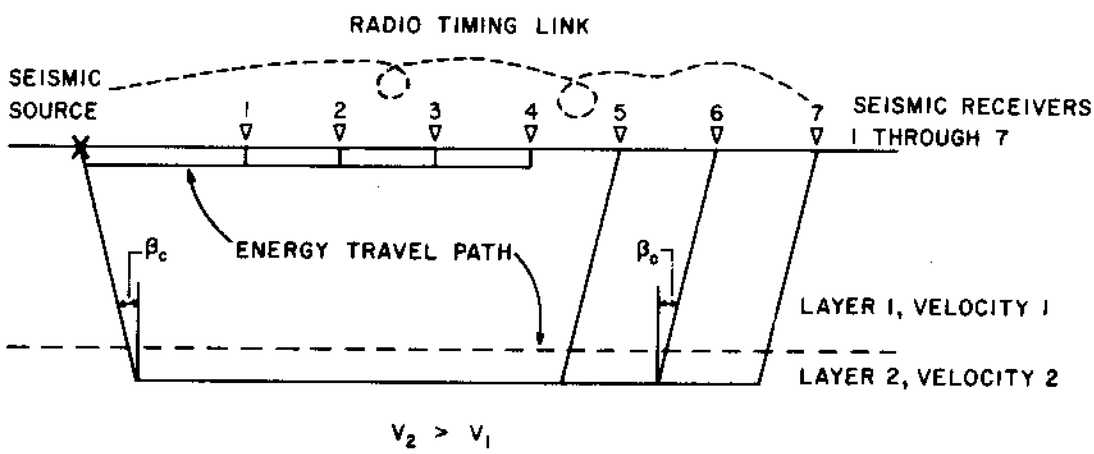

Figure 2. A sketch of an ideal two layer earth showing the ray paths from the source to receiver points 1 through 7. Note that for points 1 through 4 the first energy received at the geophones travels through Layer 1. However, for points 5 through 7 the seismic wave which travels down through Layer 1 to the geophone is faster than the direct wave which travels through Layer 1 only. Thus it is possible to determine the velocity in Layer 1, the velocity in Layer 2, the depth to Layer 2 and whether the interface between Layers 1 and 2 is sloping with respect to the surface of Layer 1. (Dobrin, 1960)

homogeneous material. However, the method is suited to large isolated inclusions and is difficult to apply when the separation distance of the inclusions is not great with respect to their average depth. Thus, using seismic refraction techniques it is possible to overlook isolated frozen materials in an otherwise unfrozen matrix. Often in these cases it is desirable to use seismic reflection methods which can clearly show the locations of subsurface point reflectors. These reflectors appear as inverted hyperbolas on an otherwise fairly uniform reflection record (Gurvich, 1972).

IV. DESCRIPTION OF SEISMIC EQUIPMENT

A six channel SIE seismic reflection/refraction system was used for most of the seismic measurements described below. The system consisted of four main units - power supply, amplifier and filter section, recording oscillograph, and master control with communication set. In addition, two twelve-volt batteries, six geophones, cabling and a blaster with a communications unit were required. The total weight of the system including a small record developing unit was approximately 500 lbs.

For most of the field work the high frequency cut-off filter and the low frequency cut-off filter were set to 230 Hz and 20 Hz, respectively. In all cases, the amplifier gains were set for the maximum tolerable level of background noise. The energy sources for the work were explosives ranging in size from one electric blasting cap for close geophone spacing to a 15 lb charge for a 728 meter line running under

Elson Lagoon (Line H, Figure 6, Line Number 27-7). Most of the lines were run with a two to five pound charge. A radio link between the seismic observer and the blaster was developed which used portable radios to provide both communication and timing for the recording system.

In addition to the SIE equipment a Bison Model 1570 signal enhancement hammer seismograph was used to obtain near surface data in a few locations to supplement the SIE records. The system consisted of an analog to digital converter, a summing amplifier, a digital memory and a cathode ray tube display with a digital read-out record-scanning cursor. The seismograph provided digital read-out of an operator-selected first-break on the geophone output waveform as well as allowing the summing of many records to enhance the received signal while averaging background noise. The extreme portability yet high degree of sophistication of this apparatus was a valuable asset to the program.

A hydrophone string using six Aqua Dyne AQ1 hydrophones with individual preamplifiers are constructed for use with the SIE seismograph. Figure 3 shows a schematic diagram and photograph of a hydrophone-preamplifier circuit in various stages of construction. The completed string was 60 meters long with a 12 meter spacing between hydrophones. Styrofoam spacers were used along the length of the cable to support it at the surface and to permit the hydrophones to float just below the water surface.

In addition to the seismic refraction equipment described above, arrangements were made to use a portable Raytheon RTT-100 acoustic

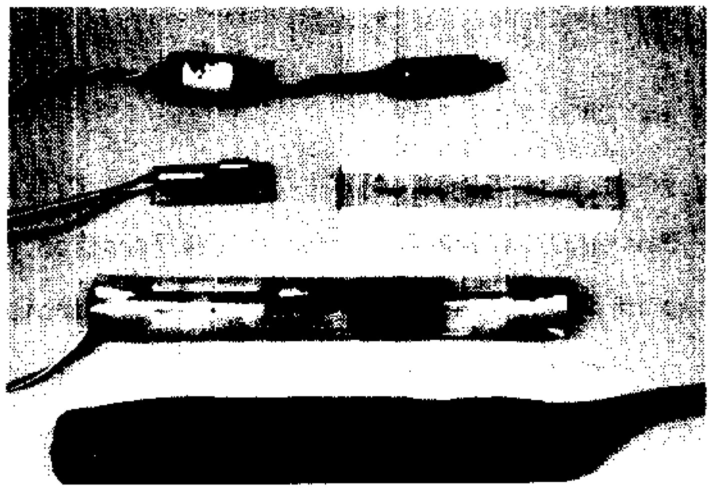

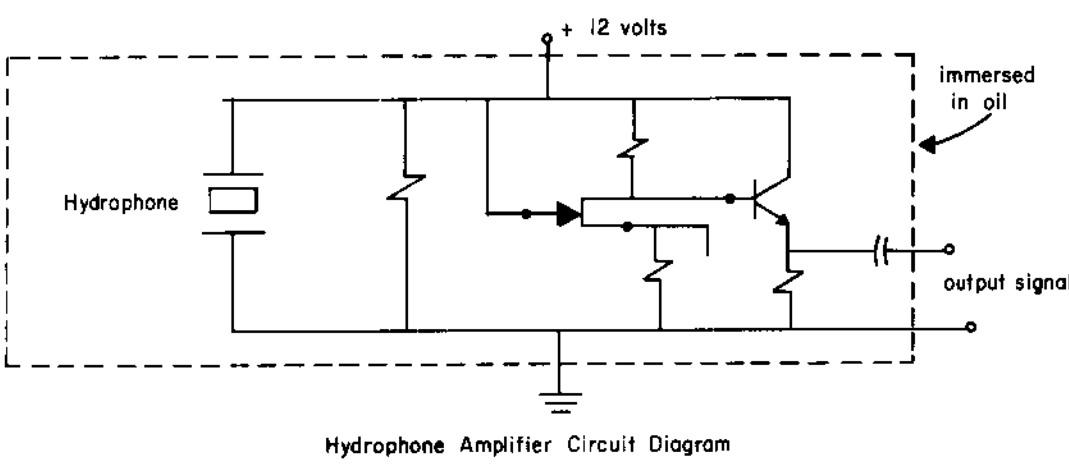

Figure 3. Circuit Diagram of Hydrophone Amplifier.

sub-bottom profiler. However, equipment difficulties necessitated sending the profiler to the factory for repairs and it was not used in the field program.

V. FIELD WORK AND DATA REDUCTION

The field program consisted of running several refraction lines in two areas near Barrow. Figure 4 indicates the location of these as "A" and "B" on a map of Pt. Barrow and vicinity. Two principal modes of transport were used for daily travel between the Naval Arctic Research Laboratory (NARL) and the field sites. All of the work at Site B was done using a 16-foot Boston Whaler with a 50 hp outboard motor for transport, while the work at Site A included use of the boat and a four-wheel drive balloon-tired truck. The duration of the field work was 14 days in late August and early September, a time marked by the absence of sea ice near the coast and maximum penetration of the thaw depth into the land surface. The first factor provided ease of boat operations. The second ensured that a surface layer with low seismic velocities would overlie any frozen material on the land, a condition necessary for seismic refraction studies (Roethlisberger, 1972).

Figures 5 and 6 show the locations of all refraction lines in the Pt. Barrow area (Area "A" of Figure 4), while Figures 7 and 8 show the lines along the Tapkaluk Islands (Area "B" of Figure 3). Details of the refraction lines are given in Table I and reversed profiles are indicated. All the travel time plots are shown in Appendix II. Note that some of the shorter lines were run in order to determine the depth to the first refracting horizon. In general, this was 2 meters or less, so that it

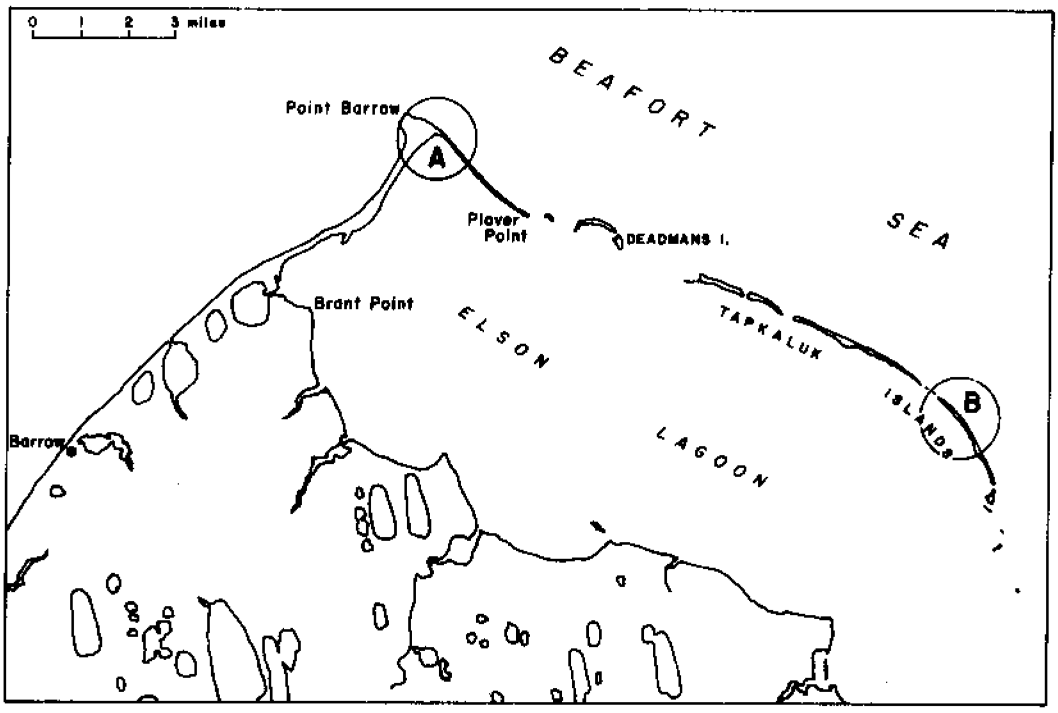

Figure 4. Map of Pt. Barrow, Alaska, vicinity. Two areas of seismic refraction studies, "A" and "B", are shown. The Barrow community is approximately 5 miles southwest of Brant Point along the coast.

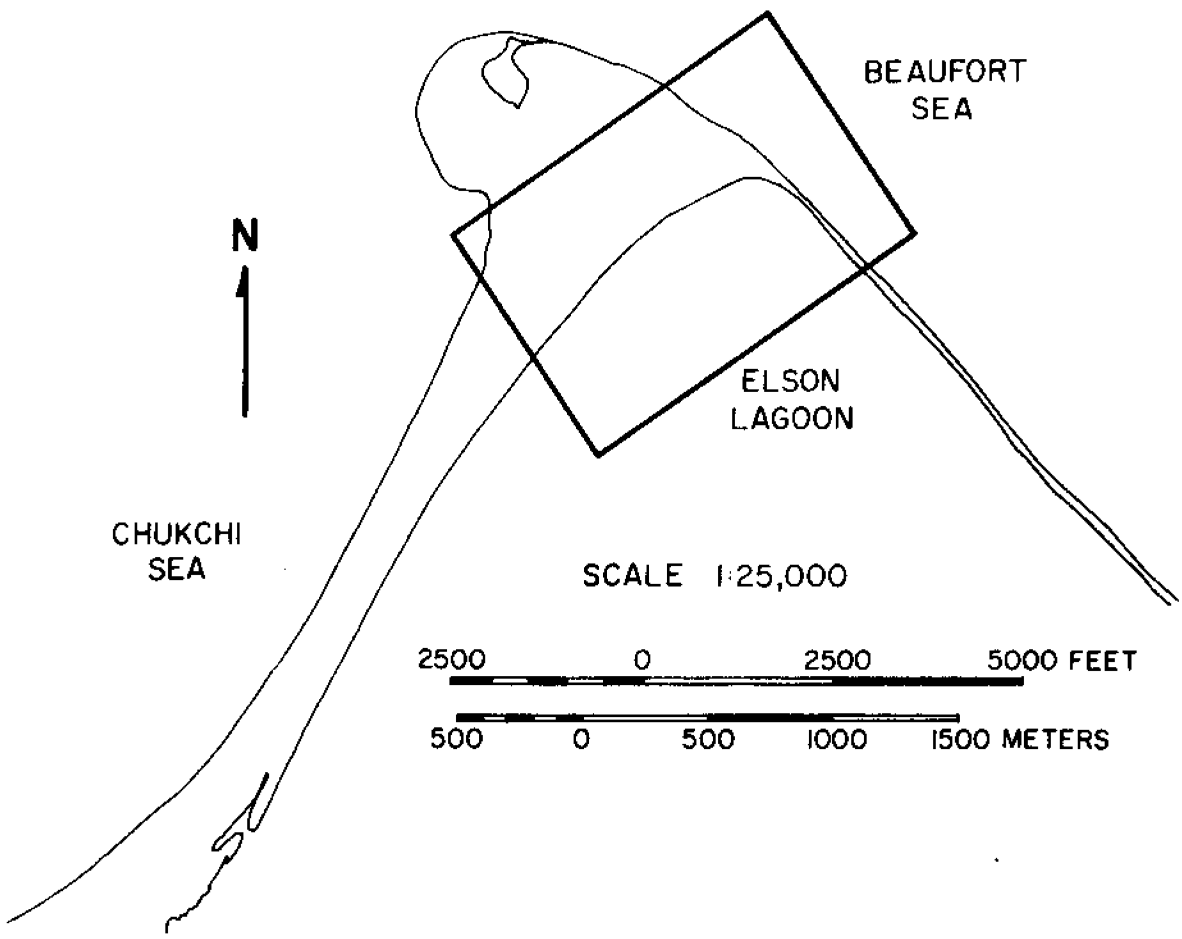

Figure 5. Pt. Barrow area (Area A of Figure 4).

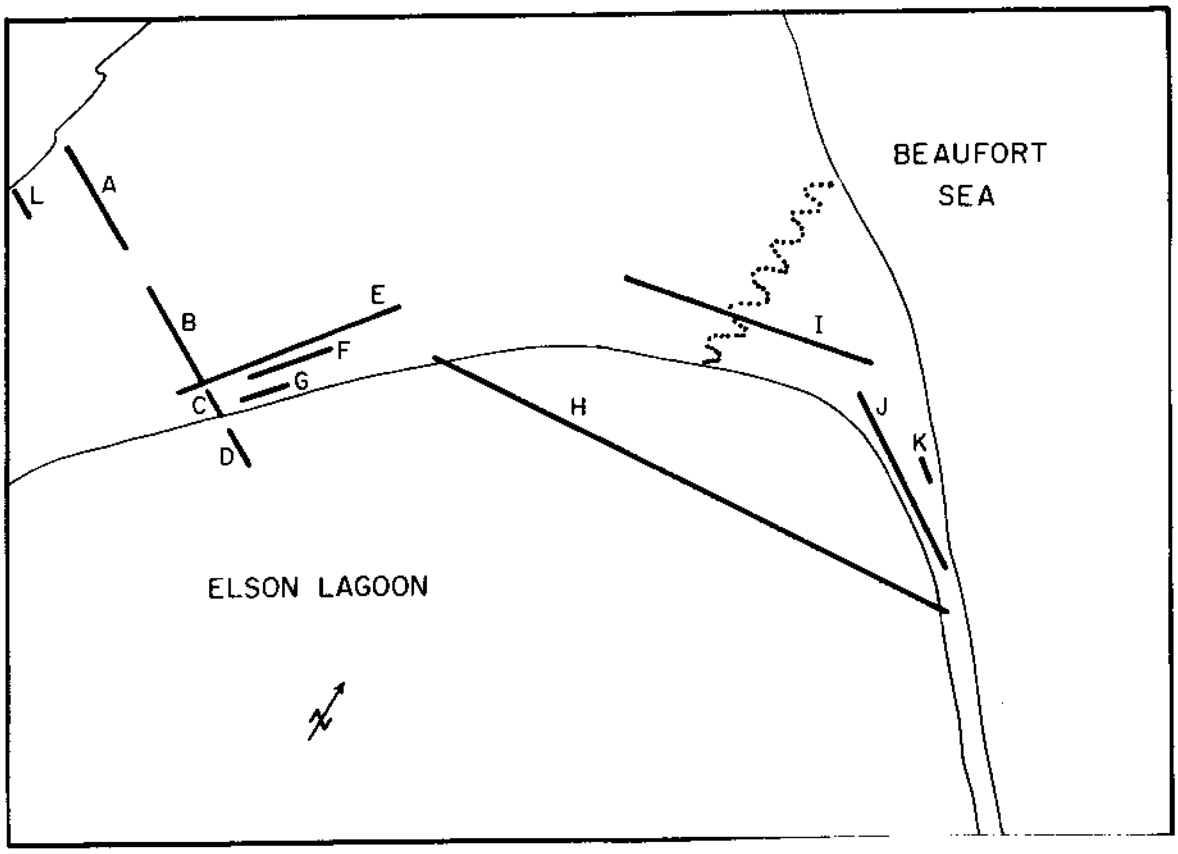

Figure 6. Seismic refraction lines in the Point Barrow area.

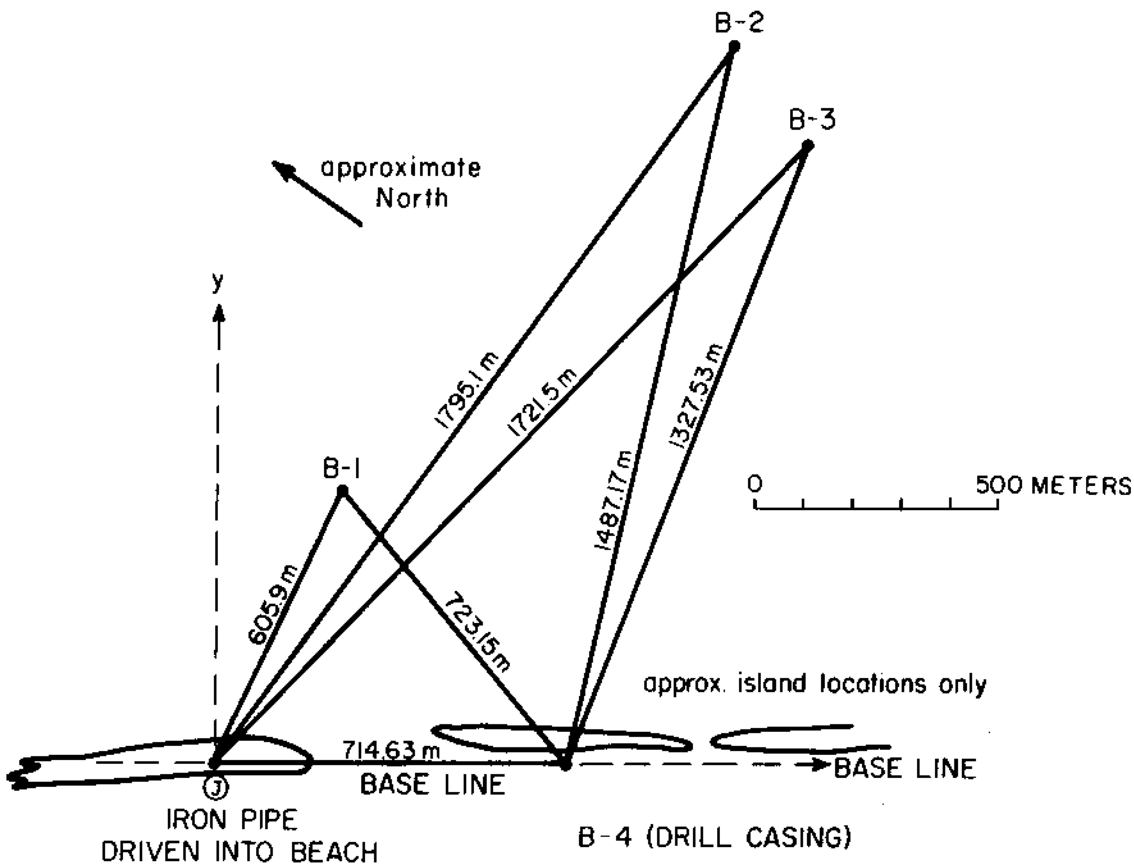

Figure 7. The Tapkaluk Island area noted as area "B" on Figure 4. Points B-1 through B-4 are locations of drill holes completed by R. I. Lewellen in the spring of 1974.

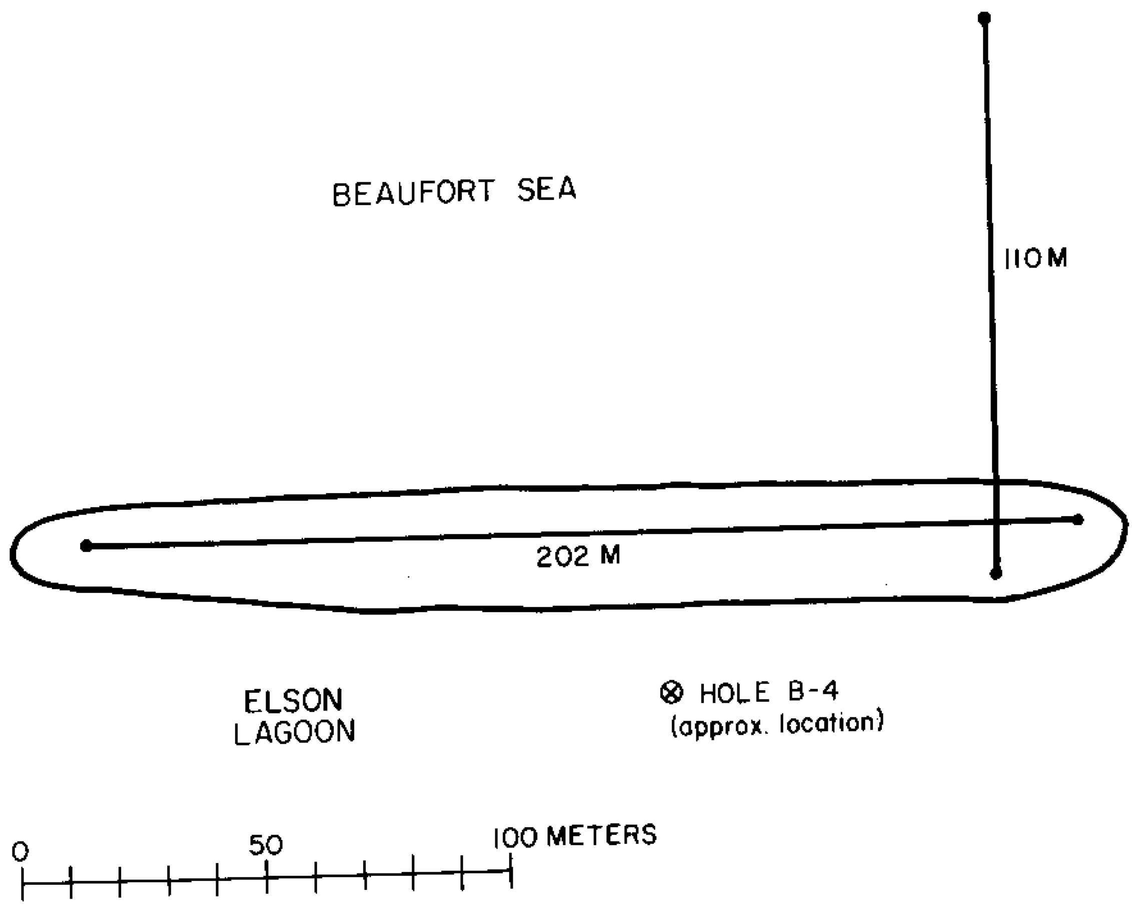

Figure 8. Refraction lines near drill hole B-4 on Tapkaluk Island.

TABLE I: REFRACTION PROFILE SYNOPSIS

Profiles utilizing explosives

Line Numbers Forward	Line Numbers Reversed	Line Letter Designator	Line Length (m)	Surficial layer velocity (m/sec) Forward	Surficial layer velocity (m/sec) Reversed	Refracting horizon velocity (m/sec) Forward	Refracting horizon velocity (m/sec) Reversed	Average depth to refracting horizon (m)	Comments
27-5 27-1 27-2	27-3 27-4	J	212	402		1844	1764	3.4	Composite reversed profile on Plover Point spit.
27-7		H	728			1773			Shot across Elson Lagoon from Barrow spit to Plover Point spit.
28-4 28-3 28-1	28-2		202	625		1654	1727	2.0	Composite reversed profile in the Tapkaluk Islands.
28-6			110	186					Anomalous -- shot from Tapkaluk Islands to hydrophones in Beaufort Sea.
29-2		K	18	312		2000		3.0	Closely spaced unreversed profile on top of Plover Point spit.
29-7 29-3	29-4	C&B	95	400		3625	2976	2.1	Composite reversed profile perpendicular to beach on southeast side of Barrow spit.
29-10	29-11	E	182			2500	2857		Reversed profile parallel to beach on southeast side of Barrow spit. Nearly complete attenuation of refraction wave beyond 120 meters.
29-7	29-9	C	16	250		2500 Dip corrected velocity	1667 1999	1.2	Closely spaced reversed profile on southeast side of Barrow spit.
30-3		D	137			1810			Water shot to beach on southeast side of Barrow spit.

TABLE I (Continued)

Profiles utilizing explosives (continued)

Line Numbers Forward	Line Numbers Reversed	Line Letter Designator	Line Length (m)	Surficial layer velocity (m/sec) Forward	Surficial layer velocity (m/sec) Reversed	Refracting horizon velocity (m/sec) Forward	Refracting horizon velocity (m/sec) Reversed	Average depth to refracting horizon (m)	Comments
30-1	30-2	C	8	690	645				Closely spaced reversed profile partly in water on southeast side of Barrow spit.
30-6	30-5	A	105			2986	2903		Reversed profile on northwest side of Barrow spit.
Profiles utilizing hammer seismograph									
10-1 11-1 12-5	11-2 12-6	A L	40 30						Top of Barrow spit and Chukchi Sea side of Pt. Barrow. Velocities and arrival times very anomalous, indicating subsurface lenses of high velocity and limited extent (see figures).
11-3	11-8	F	50,30	1608	1744	3000	3290	1.9 2.5	Partially reversed profile near concave site of Barrow spit parallel to beach (approx. 18m to beach).
11-4	11-5	"C"	15	830	1440	2949	2883	1.1 2.1	Reversed profile near concave side of Barrow spit perpendicular to beach near C.
11-6	11-7	"G"	30	1815	1063	2842	2910	2.9 1.7	Reversed profile on southeast side of Barrow spit parallel to beach (approx. 12m to beach).
11-9 11-10 11-11		I I I	30 30 30			1970 1683 2857			Profiles near concave side of Barrow spit. Velocities increase from east to west (see figure 10).
12-1 12-2 12-3 12-4		I I I I	30 30 30 30			2600 2800 2778 1739			Same as above
Meat Celler			10			2535			Representative velocity in known permafrost terrain.

was necessary to reduce the spacing of the geophones in order to sample the velocity in both layers with the same shot. The lines are generally identified by number and letter designation. The number designator indicates the specific data plotted in Appendix II while the letter designator indicates the refraction lines shown in Figure 6.

The baseline indicated in Figure 7 was established on May 23 while the last of Lewellen's holes (hole B-4) was being drilled. The location of all the holes was established with electronic distance measuring equipment and a theodolite. The reference base line is marked by the casing for hole B-4 and an iron pipe driven 70 cm into the island (Illustration I). Appropriate distances are also shown in the figure. Area "B" on Tapkaluk was not located using surveying techniques. Instead, the weasel odometer was calibrated using the distance measuring equipment. Following this the distance from Plover Point to Site "B" was measured while traveling over the lagoon ice with the odometer. This provided good location information for the summer work with the boat, as the drill casing for B-4 and the iron pipe were both easily located using Plover Point as a starting point and the island chain for direction. In late August, hole B-4 was located in about 50 cm of water at approximately 40 meters from the shore of Tapkaluk Island in Elson Lagoon (Figure 8).

Although the summer reconnaissance of the island indicated, on the whole, a continuous island of low relief (at most perhaps 1.5 meters above the sea water), the island by Site B had two passages through it (Figure 7). The most easterly of these was at most 30 cm deep while the most westerly one was perhaps as deep as 45 cm. These provided a pass-

Illustration I. (a) Balloon-tired vehicle used on grassy portion of Pt. Barrow spit. (b) Stake driven into the fine gravel of Tapkaluk Island. Note total absence of vegetation.

age for Lewellen's drill sled through the small linear ice pile found along the Beaufort Sea side of the island in the spring of 1974.

In addition to the two areas shown in Figure 4, several data points were taken in the walls of the NARL animal colony meat cellar, an excavated room approximately 12 meters below the tundra surface at the camp. The walls, separated by about 5 meters, generally consisted of sand containing small shells with some cross-bedded coarse sand at different elevations. As indicated in Table I the velocity measured in the ice-bonded walls was 2535 m sec^{-1}, a value seen in the next section to be near the lower bounds of the ice-bonded permafrost velocities.

VI. RESULTS AND CONCLUSIONS

If we neglect the low velocities of the surficial layer shown in Table I, which are typically about 200 to 400 m sec^{-1}, we can separate the refracting horizon velocities into two groups. The first group contains velocities of 2000 m sec^{-1} and less while the second group contains velocities greater than or equal to 2500 m sec^{-1}. Figure 9, a plot of all refracting horizon velocities, clearly indicates the two categories. Investigations with hand augers indicate the high velocity group is associated with ice-bonded permafrost while the low velocity group is associated with non ice-bonded material.

For those lines along which no velocities typical of ice-bonded permafrost were detected, it is possible to estimate from the seismic data the minimum depth to the top of such a layer if it existed, but were beneath the penetration depth of the first arrival energy. The calculation, given in Appendix I, is based upon a conservative velocity estimate for the suspected fast layer of 2400 m sec^{-1}, a value lower

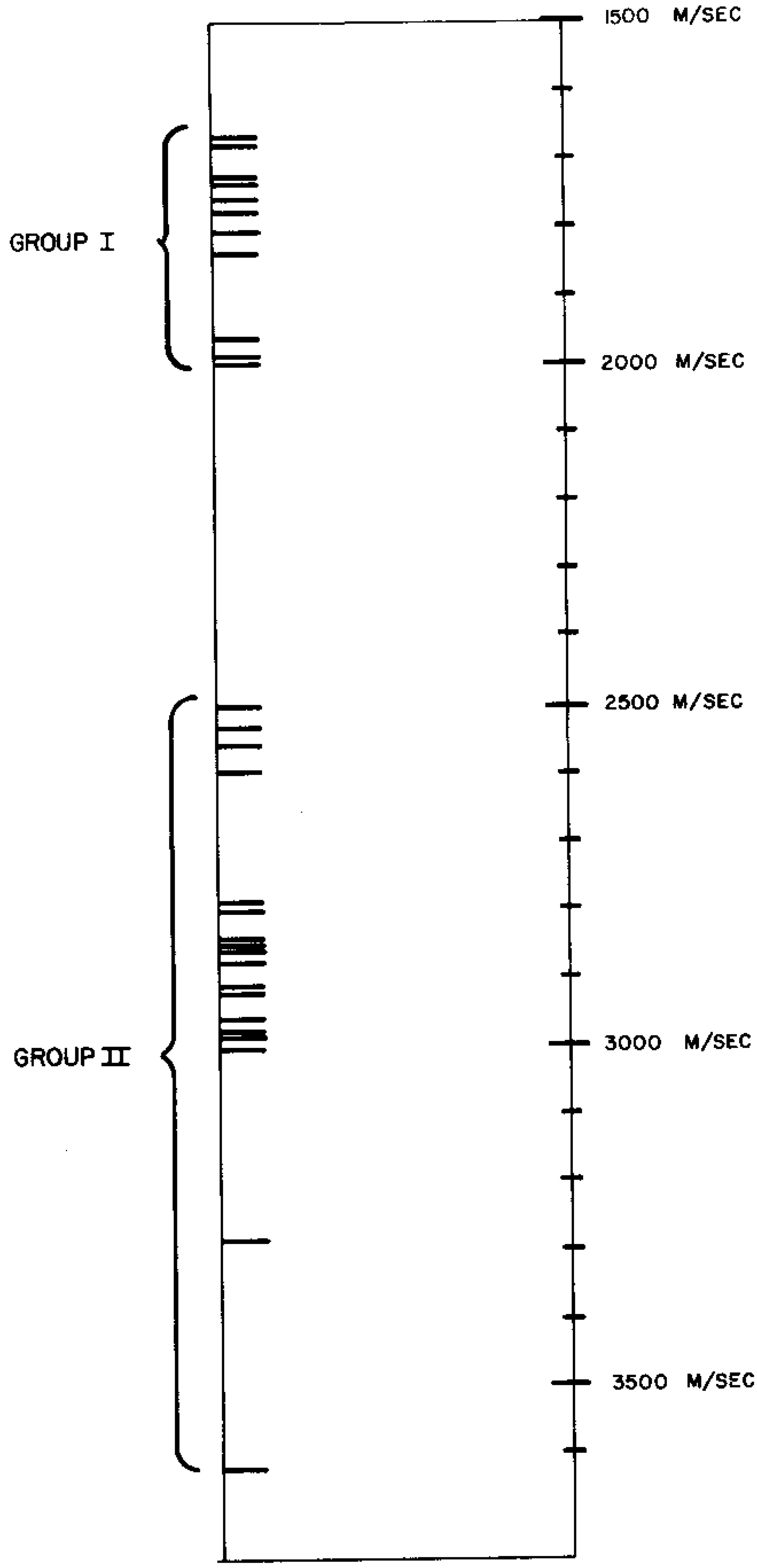

Figure 9. Seismic velocities of the refraction layer (taken from Table I, Column 4). Group I is indicative of non-ice bonded materials while Group II is indicative of the ice-bonded permafrost.

than any of those found in group 2 of Figure 9. It is seen from the calculation that the minimum depth to the first layer is 0.22 times the length of the refraction line. Since a comparatively low velocity was assumed for the frozen layer, the depth estimate probably represents an absolute minimum for the investigation area.

A boundary, indicated in Figure 6 as a wavy line running approximately north to south, separates the older land area southwest of the point from the sand spit leading to Plover Point to the southeast. The distinction between these terrains is obvious in the field from the presence of scattered vegetation on the west side of the boundary and the evidence of southward migration of the spit with concurrent burial of the vegetation surface by sand and gravel. Illustration I portrays the difference between the lightly grass-covered portions of the spit west of Pt. Barrow and the barren terrain found on Plover Point spit and Tapkaluk Island.

The approximate boundary in Figure 6 also marks the eastern limit of occurrence of ice-bonded permafrost in the subsurface as determined from the seismic data (see Figure 10, line I). None of the lines along the spit to Plover Point (J, K and east half of I), the Tapkaluk Islands (Figure 8), or the long shot across the northwest corner of Elson Lagoon (line H in Figure 6) encountered velocities typical of this material. However, all seismic data taken to the east of this boundary indicate high velocity refractions with the exception of line D. Figure 10 illustrates the abruptness of the transition on line I from relatively high velocities to lower velocities characteristic of non ice-bonded material.

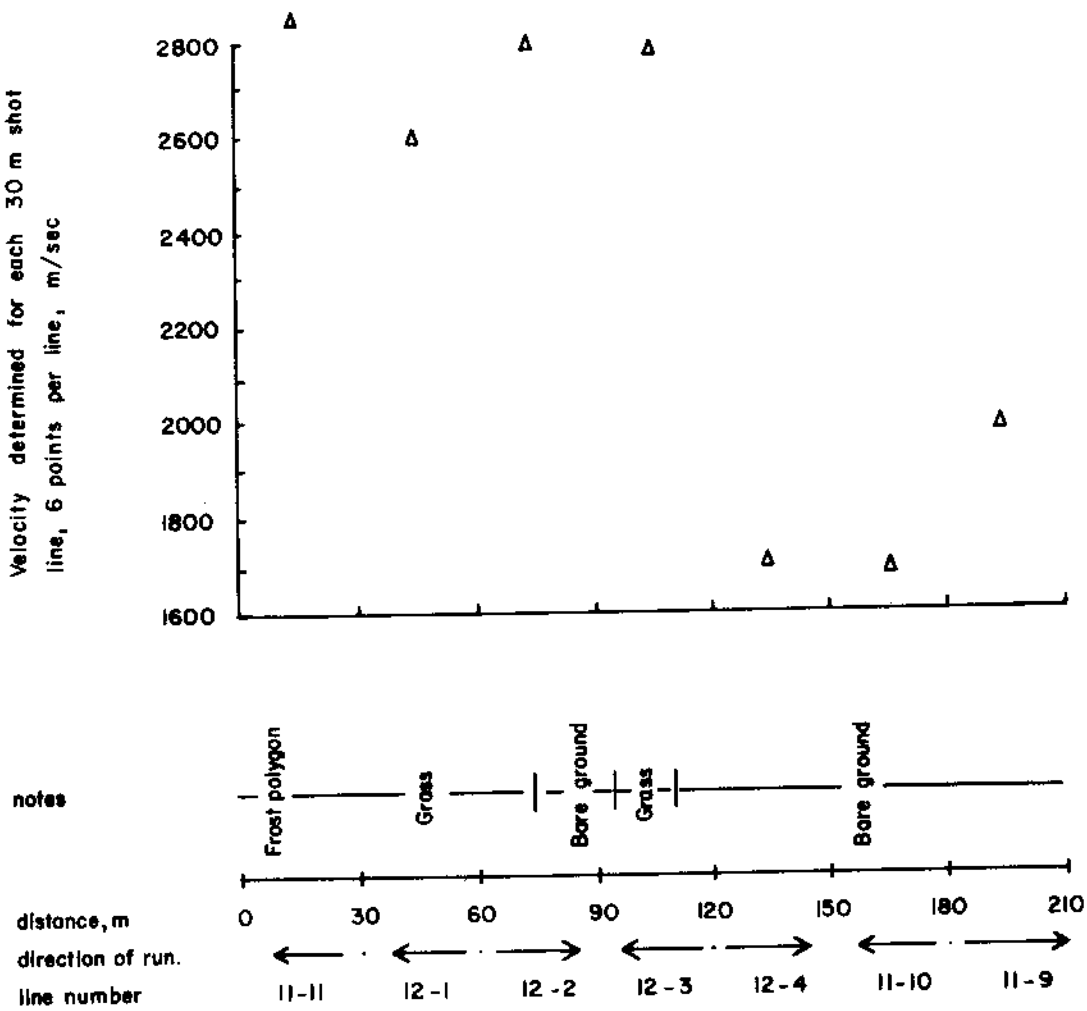

Figure 10. The seven seismic lines that make up line I of Figure 6. Line 11-11 is the most western portion while Line 11-9 is the most eastern portion of Line I. The approximate transition from vegetated to barren ground is seen to coincide approximately with the transition from high velocities (frozen) to low velocities (not frozen).

From the seismic data, the depth to the top of the ice-bonded permafrost surface west of the boundary was about 1.5 to 2 meters over most of the area south of Pt. Barrow. This was checked by probing at a few sites, and, in addition, two small samples of the permafrost were collected using a SIPRE corer (Illustration II). In both instances, the ice was fresh. However, this cannot be taken as proof that the ice is fresh throughout. It is possible that the ice bonding most of the permafrost in the area is saline, and that the fresh ice represents rainwater or snowmelt which has percolated down through the porous gravels to the top of the permafrost and frozen. There is an obvious need for shallow drill holes to determine which alternative is correct.

One important result of this study comes from the interpretation of several lines on the shore of Elson Lagoon south of Pt. Barrow. Line B of Figure 6 is a reversed profile extending inland from the lagoon for 95 meters. The data from this line show the presence of a continuous surface with the velocity of ice-bonded permafrost, at a depth of about 2.1 meters. A short line, line C, was run to extend the longer line to the water's edge but failed to detect any fast zone. Finally, a single shot to the same array from a point 135 meters offshore gave a velocity of 1810 m sec^{-1} (line D). These results show that the surface of the ice-bonded permafrost must drop off rapidly near the water's edge. Assuming the fast layer is parallel to the bottom of Elson Lagoon and deeper than the detection depth, the calculations in Part II of Appendix I give a minimum depth to the refractor of 30 meters. If, however, it is assumed that the fast layer is planar and dips toward the lagoon with respective slow layer and fast layer velocities of 1800 and 2400 m sec^{-1}, one can calculate a minimum depth to the interface at the south

Illustration II. SIPRE auger used to obtain frozen samples from shallow depths southwest of Pt. Barrow.

Illustration III. Plover Point end of Line H.

end of line D. Such a calculation gives a minimum depth to the fast layer of about 68 meters with an interface slope of approximately 30°. (The water depth, 2 meter maximum, has been ignored and the depth to the bonded permafrost on the north end of line D is assumed to be about 2 meters, a value comparable to that found for line G.) Thus, if bonded permafrost exists beneath Elson Lagoon at line D, it must be deeper than a plane dipping toward the south at an angle of 30° with respect to the horizontal. Further, applying the conservative parallel interface approximation to line H, the minimum depth to the fast layer is 160 meters. This figure is considerably greater than the depths of approximately 60 to 100 meters observed in the Canadian islands by Hunter and Hobson (1975). We conclude that, although sub-bottom temperatures below 0°C have been reported in the west end of Elson Lagoon to depths of 12 meters (Lewellen, 1974), these temperatures are not associated with continuous ice-bonded permafrost.

Although isolated ice-bonded permafrost cannot be ruled out along line H, it is apparent that only a small percentage of the 728 meter line could contain bonded material. Such a conclusion is based upon the fact that the average velocity observed (1773 m sec^{-1}) is typical of the non ice-bonded material in this area and is significantly less than the minimum velocities observed in ice-bonded permafrost (2500 m sec^{-1}).

In addition to the work near Pt. Barrow discussed here, the island near which Lewellen drilled four holes last spring was visited, and his last hole was easily located (the region corresponds to area "B" in Figure 4). A refraction profile 230 meters long was run along the axis of the island (Figure 8) yielding 1700 m sec^{-1}, a velocity associated with non-bonded materials. Thus, we conclude there is no continuous permafrost within 50 meters of the surface at that location. Further, the uniformity of Tapkaluk Island suggests this conclusion can be extended to Plover Point.

Shearer et al. (1971) discuss their observations of submarine pingos in the Beaufort Sea. They conclude the pingo-like features mapped near the mouth of the MacKenzie River were formed under the ocean prior to 5000 years ago after a major oceanic transgression. They further point out that the present temperatures measured at the sea bed, -1°C to -1.8°C, can be expected to freeze any fresh interstitial water in the sea bed. However, this is most likely in the presence of relatively impermeable clays which will prevent sea water from mixing with the interstitial water.

The continuous high rate of beach erosion, redeposition, and the transitory nature of the barrier islands suggest that sea water brines are probably present to great depth beneath the sea floor here. This is particularly likely with the rather coarse gravel and sand found in the Barrow area. Such material could indeed be a few degrees below 0°C and still not be ice-bonded. A significant conclusion is that the burial of sub-sea pipelines (hot oil pipelines, perhaps) will not be seriously impeded by ice-bonded permafrost in these seabed conditions, nor will elevation of permafrost temperatures (using the classic definition for permafrost) present a mechanical hazard.

Present estimates of the shape of the permafrost surface along the boundary of Elson Lagoon at the Barrow spit are speculative at best. If this is a well-defined boundary (a subject for further speculation) it may extend under Elson Lagoon with a dip angle of greater than 30° or, alternatively, it may reverse and dip back under the spit as illustrated in Figure 11. Additional refraction profiles along the boundary coupled with selected shallow drilling would serve to further define the interface.

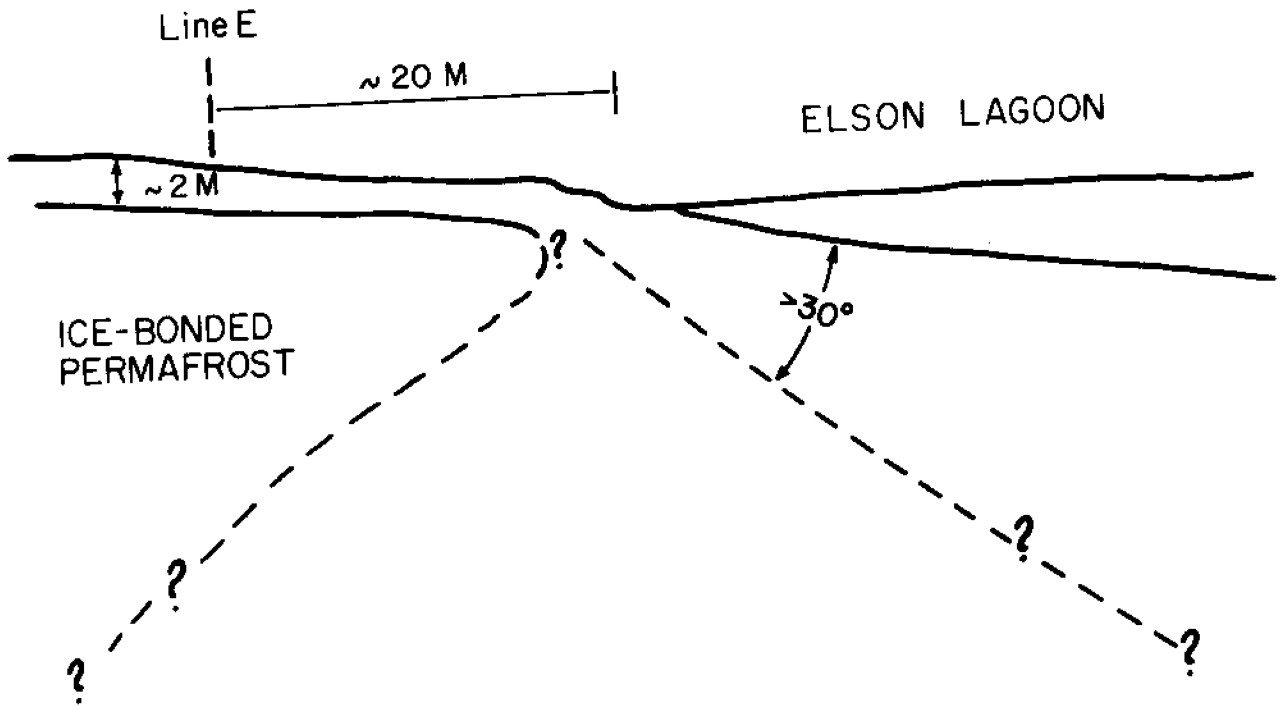

Figure 11. Possible permafrost boundary configuration at the edge of Elson Lagoon (line D, Figure 6).

SECTION B

THERMAL STUDIES

I. EXPERIMENTAL WORK

Early in 1974 we decided to concentrate our experimental efforts in cooperation with the instrumentation and sample analyses in a drilling project proposed by Lewellen. Since no samples were obtained from him, we performed our studies on near surface samples which we obtained by hand drilling. In addition, the instrumentation for long term temperature measurement in off-shore drill holes was developed.

A. Laboratory and Field Work

After it became apparent that it would not be possible to obtain core material from Lewellen's drilling program promptly, an attempt was made to obtain some frozen ground and permafrost core from a land site near NARL. The purposes for obtaining such core were to test the effectiveness of the SIPRE ice corer in silty frozen ground and to obtain frozen core which could be used to test our laboratory techniques and apparatus for structural, thermal and physical analysis of these cores.

The SIPRE ice corer was operated by hand and also with a standard power unit (5 HP gasoline engine). When the corer was operated by hand it was found that the cutting teeth clogged in the same way as when coring in ice at the melting point. This prevented us from obtaining good cores by hand; however, in the same soil it was found that the motor driven corer operated satisfactorily. It appears that a certain minimum rotation speed is necessary for the chips to be carried out of the hole.

Two cores have been obtained from the Footprint Creek area (IBP site) near NARL. The cores were maintained in a frozen state and shipped to the Geophysical Institute where they were stored at -25°C. Two more cores were obtained from near the animal colony in the NARL camp area. In addition to these cores, some pieces of frozen ground and permafrost have been obtained from Point Barrow and from the underground meat cellar at NARL. One of the cores was used to further develop* our structural analysis technique using thin sections and the other three cores are stored in a freezer and will be used to develop techniques and apparatus for thermal and physical analysis of frozen cores.

Many thin sections of core (a few tenths of a millimeter in thicknesses) were cut and photographed under crossed polaroids. A representative photograph is shown in Figure 12. This photography clearly shows the location, size and distribution of ice lenses in the frozen ground.

A literature search was conducted to obtain information on the thermal parameters of frozen ground and permafrost. This search is about 60% complete. In addition, experimental techniques for measuring the thermal conductivity and thermal diffusivity were evaluated. Due to our requirements (low precision, simplicity and convenience), it was decided to forego construction of a precise thermal conductivity apparatus and to use a thermal conductivity probe instead. For the same reasons, a less precise but relatively fast and simple technique was selected for measuring the thermal diffusivity. This technique uses a 3 inch diameter core in a specially designed cold chamber. The outside of the core is driven with a sinusoidal thermal wave and the temperature is measured at the edge and center of the core. The thermal diffusivity can then be computed both from the ratio of the amplitudes of the temperature waves at the end and in the center of the core, and from the difference in

---

*This development work was supported by the Office of Water Resources Research, Project Number C-4049.

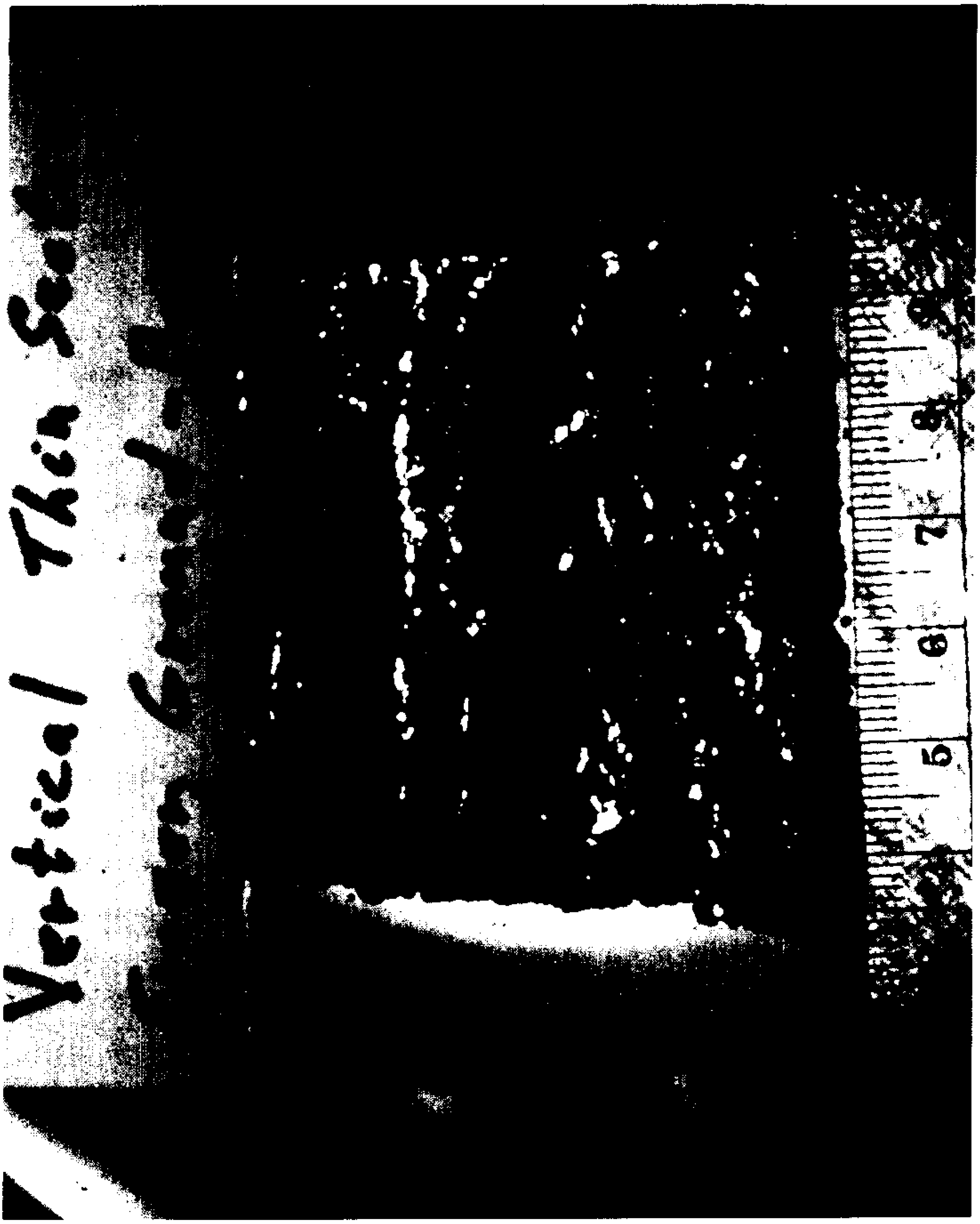

Figure 12. Thin section of permafrost core showing ice lenses.

phase of the two thermal waves (Carslaw and Jaeger, 1959). We intend to use the amplitude analysis method. To date, the specially designed cold chamber has been constructed, and some of the associated electrical equipment has been ordered.

B. Temperature Measurement in Offshore Drill Holes

Based on our observations of Lewellen's drilling, and on our own experience with the measurement of temperature and physical properties in glacier ice (Harrison, 1972; Harrison and others, 1973; Trabant and others, 1973; Harrison, 1975; Raymond and Harrison, 1975), we have drawn some conclusions concerning temperature measurement in the offshore region. It appears to be rather difficult to get undisturbed temperatures in a short-term experiment. Attempts at driving a temperature probe into undisturbed material at the bottom of a drill hole may be complicated by the migration of material into the bottom of the hole. In order to obtain a good estimate of the equilibrium temperature after the disturbance has been introduced, temperature measurements must be made for a time greater than that during which heat from the disturbance is released (Bullard, 1974; Lachenbruch and Brewer, 1959). This time could easily be months in the case of latent heat released by sea water slowly freezing in a hole enlarged by caving. Therefore, long-term temperature measurements will often be necessary for good accuracy to be achieved. Of course, real temperature variations with time are also of interest. Further information will be available in Lewellen's report.

At the same time, recovery of an offshore bore-hole in ice-infested waters for temperature measurement presents obvious problems. The hole can be backfilled with diesel fuel and re-entered periodically, as is sometimes done on land, or a thermistor cable can be permanently placed in the hole. We chose the latter approach. Problems of sealing the cable against corrosion and water have been solved by oceanographic equipment manufacturers, and a suitable commercially available cable was found. Specifications are given in Appendix III. This particular cable is 50 meters long and has thermistors at 5 meter intervals. Because the thermistors used are "interchangeable", calibration at one temperature is adequate for most purposes. This was done by placing the entire cable in a carefully prepared ice bath. The results, which have absolute accuracy of about 0.005°C, are also listed in Appendix III.

A simple cable recovery system was devised and constructed. A special termination flange on the thermistor cable is connected to a weight with a short length of line. A small float is connected to the weight with a second length of line which is adjusted so that the float remains beneath the depth of the thickest ice expected. Careful surveying allows the site to be recovered; this is judged to be easiest early in winter when the ice is still thin and a hole can be easily cut, enabling the float to be recovered with a simple fishing tool. This system will not work where the ice freezes to the bottom, or where it grounds.

A cable deployment system was built after consultation on its feasibility with Lewellen. The cable is designed to be placed in a borehole and the casing pulled around it. Following this, a simple device designed to prevent the cable from slipping down the borehole is attached to the cable, slid down it, and clamped around it at the level of the ocean bottom. This deployment can be done through a hole in the ice.

The cable and associated systems were prepared and made available to Lewellen in Barrow in the spring of 1974, but were not placed in any of the drill holes during the drill season. See his report for further details.

II. THEORETICAL WORK

The apparent absence of frozen ground under Elson Lagoon inside Barrow spit has led us to consider the physics of how frozen ground might thaw from the top after a transgression of the ocean. When the ocean bottom temperature is negative, which may be typical of Alaska's northern coast, conventional thermal conduction models are not applicable. The question of how deep the ground is thawed near shore is a problem of interest, and an understanding of the processes involved will enable predictions to be made over wide areas where no field data are available.

Consider first the case in which the frozen ground is pure ice, covered suddenly with sea water at -1°C and a salinity corresponding to a freezing point of -1.8°C. If water temperature and salinity are kept fixed by constant replenishment the ice will melt extremely rapidly because of the salt. For this reason one would not expect to find ice at the ocean floor except under special conditions, such as when the sea ice freezes to the bottom or where the shore has very recently retreated.

In practice, frozen ground contains material other than ice, and in these materials temperature and salinity gradients can be set up which retard the melting. The transport of salt is the key to this problem, and probably the rate controlling process. Obviously several different mechanisms of salt penetration are possible. The simplest is the transport of salt purely by the mechanism of molecular diffusion into ground initially salt free. We consider a situation in which geothermal heat flow is neglected, along with the heat capacity of the ground. These approximations would be valid for fairly short times after ocean transgression, and for ground of reasonably high ice content. This gives a Stefan-type problem, the solution of which can be found in closed form; mathematical details are given in Appendix IV.

One finds that the thickness X of thawed ground increases as the square root of the time t after ocean transgression:

$$X = (p\ \sqrt{4\kappa_s})\ \sqrt{t} \tag{1}$$

where the general form of the constant p, which depends upon the thermal properties, the ice content, and the diffusivity of salt in the thawed ground κ_s, is also given in Appendix IV. We assume that the following rough but not unreasonable numerical values apply:

κ_s (bulk diffusivity of salt in the thawed ground)	$\approx 1 \times 10^{-6}\ cm^2\ sec^{-1}$
T_f (freezing point of seawater)	$\approx -1.8°C$
T_o (mean annual ocean bottom temperature)	$\approx -1.0°C$
K (thermal conductivity of thawed ground)	$\approx 0.005\ cal\ sec^{-1}\ cm^{-1}\ deg^{-1}$
h (latent heat per unit volume)	$\approx 20\ cal\ cm^{-3}$

(This value of h would be appropriate for ground of about 25% ice content.) Then it is found that to a good approximation (Appendix IV) the constant p is given by

$$\sqrt{\pi}\ p\ e^{p^2}\ \mathrm{erf}\ p \approx \frac{T_f}{T_o} - 1, \tag{2}$$

or $p \approx 0.57$. The thickness of thawed ground would increase as follows:

Time	Thickness
0	0
1 year	0.06 m
10	0.2
100	0.6
1,000	2
10,000	6

When the ocean bottom temperature is positive and $\frac{KT_o}{h\kappa_s} >> 1$, the theory reduces to $X \approx \left(\sqrt{\frac{2T_oK}{h}}\right)\sqrt{t}$ which is the result of conventional Stefan theory.

Equations (1) and (2) imply that for a bottom temperature which is significantly negative (as is probably the case along most of the Arctic coast), to a good approximation the rate of thawing from the top in this model does not depend upon the thermal properties or ice content at all. It follows that experiments which measure only those properties may shed little light on the process of thawing from the top.

This simple picture neglects the effect of geothermal heat, the effect of the soil on the melting point of its H_2O, the presence and motion of salt in the frozen ground, heat capacity, and most importantly, the effect of liquid motion. Nevertheless, it illustrates the basic idea - the importance of processes other than the conduction of heat - fairly well. We are now investigating models which remove these restrictions in order to determine the observable consequences.

ACKNOWLEDGMENTS

The work described in this report was supported by NOAA, Office of Sea Grant, Department of Commerce, under Grant No. 04-3-158-41. Also, the Alaska Oil and Gas Association (AOGA) provided financial support and a portion of the core analysis work was supported by the Office of Water Resources, Project No. C-4049. The State of Alaska, Department of Highways, provided the hammer seismograph. The Office of Naval Research, Naval Arctic Research Laboratory, was the support base for the field work. The support of these organizations is gratefully acknowledged.

REFERENCES

Anderson, D. M., A. R. Tice and H. L. McKim, 1973. The unfrozen water and the apparent specific heat capacity of frozen soils, Permafrost, 2nd Int. Conf.

Bell, D. L., W. J. Porter, A. S. Westneat, 1973. Progress in the use of acoustics to classify marine sediments. Ocean 73, IEEE Publication 73 CH0774-0 OCC.

Bullard, E. C., 1947. The time necessary for a borehole to attain temperature equilibrium. Monthly Notices of the Royal Astronomical Society, Geophysical Supplement, Vol. 5, No. 5, p. 127-130.

Carslaw, H. S. and J. C. Jaeger, 1959. Conduction of heat in solids. Second Edition Oxford, Oxford University Press.

Dobrin, M. B., 1960. Introduction to Geophysical Prospecting. McGraw-Hill.

Ferrians, O. J., Jr., G. D. Hobson, 1974. Mapping and Predicting Permafrost in North America: A Review. 1963-1973 Permafrost, 2nd Int. Conf.

Ferrians, O. J., Jr., 1965. Permafrost Map of Alaska. U. S. Geological Survey, Misc. Geol. Inv. Map I-445, Scale 1:250000.

Gurvich, I., 1972. Seismic Prospecting. MIR Publishers, Moscow.

Harrison, W. D., 1972. Temperature of temperate glacier. J. Glaciology, II(61), 15-29.

Harrison, W. D., R. L. Mayo and D. C. Trabant, 1973. Temperature measurements on Black Rapids Glacier, Alaska, 1973. Proceedings of the Alaska Science Conference, in press.

Harrison, W. D., 1975. Temperature measurements in a temperate glacier. J. Glaciology, in press.

Hobson, G. D., 1962. Seismic exploration in the Canadian Arctic islands. Geophysics, 28(2).

Hunter, J. A. M. and G. D. Hobson, 1974. A seismic refraction method of detecting sub-sea bottom permafrost. Beaufort Sea Symposium Proceedings, San Francisco, AINA.

Hunter, J. A. M., 1974. The application of shallow seismic methods to mapping of frozen surficial materials. Permafrost, 2nd Int. Conf.

Johnson, P. R. and C. W. Hartman, 1969. Environmental Atlas of Alaska, University of Alaska.

Lachenbruch, A. H., 1957. Thermal effects of the ocean on permafrost. Bull. Geol. Soc. Am., 68.

Lachenbruch, A. H. and M. C. Brewer, 1959. Dissipation of the temperature effect of drilling a well in arctic Alaska. U.S. Geological Survey Bulletin, 1083-C, 73-109.

Lewellen, R. I., 1974. The occurrence and characteristics of newshore permafrost, Northern Alaska. Permafrost, 2nd Int. Conf.

McGinnis, L. D., K. Nakao and C. C. Clark, 1974. Geophysical Identification of frozen and unfrozen ground, Antarctica. Permafrost, 2nd Int. Conf.

Palowicz, E. F., 1971. Ocean engineering significance of marine seismic reflection profiling technology. Naval Civil Engineering Laboratory, Port Hueneme, AD724674.

Raymond, C. F. and W. D. Harrison, 1975. Some observations on the liquid and gas phases in temperate glacier ice. J. Glaciology, accepted for publication.

Roethlisberger, H., 1972. Seismic exploration in cold regions. CRREL Science and Engineering Monograph II-A2a.

Sellman, P. V. and J. Brown, 1974. Stratigraphy and diagenesis of perenially frozen sediments in the Barrow, Alaska region. Permafrost, 2nd Int. Conf.

Shearer, J. M., R. F. Macnab, B. R. Pelleiter and T. B. Mith, 1971. Submarine pingos in the Beaufort Sea. Science, 174.

Trabant, D., W. D. Harrison and C. S. Benson, 1973. Thermal regime of McCall Glacier, Brooks Range, Northern Alaska. Proceedings of the Alaska Science Conference, in press.

APPENDIX I

THE SEISMIC REFRACTION TECHNIQUE

A. TWO LAYER EARTH MODEL

Figure 2 (reproduced here as Figure A-1 for convenience) illustrates the principle of seismic refraction. Two distinct layers are shown: the thawed active layer and the ice-bonded permafrost below. Note that the method works only if the velocity in the lower layer is greater than the upper layer (Roethlisberger, 1972). Fortunately, this is the case for a thawed active layer above frozen permafrost (Hobson, 1962). Also, in the multi-layer situation of water overlying unfrozen sediment which in turn overlies frozen sediment, it is possible to identify the faster velocities associated with the frozen material (Hunter and Hobson, 1974). In general, two different types of waves are analyzed in seismic work: body waves and boundary or surface waves. In most seismic refraction work the surface waves can be ignored because they propagate slowly compared to the body waves. Further, there are two types of body waves, compressional-dilatational waves, or P waves, and shear waves, or S waves. The P waves are faster and are used exclusively for refraction work utilizing first arrival energy to determine velocities (Roethlisberger, 1972). In this report we restrict ourselves to first arrival energy and are therefore concerned only with P waves.

Note that paths 5, 6 and 7 all intersect and leave layer 2 at the same angle, β_c, with respect to the normal. This angle, called the critical angle, can be determined from Snells Law if one knows the velocity in layer 1 (ν_1) and the velocity in layer 2 (ν_2):

$$\sin \beta_c = \frac{\nu_1}{\nu_2}$$

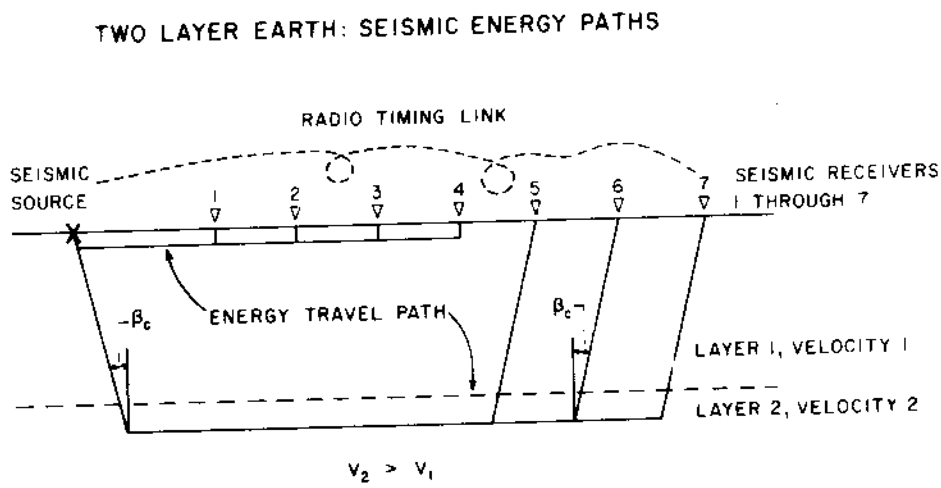

Figure A-1. A sketch of an ideal two layer earth showing the ray paths from the source to receiver points 1 through 7. Note that for points 1 through 4 the first energy received at the geophones travels through Layer 1. However, for points 5 through 7 the seismic wave which travels down through Layer 1 and along Layer 2 before ascending through Layer 1 to the geophone is faster than the direct wave which travels through Layer 1 only. Thus it is possible to determine the velocity in Layer 1, the velocity in Layer 2, the depth to Layer 2 and whether the interface between Layers 1 and 2 is sloping with respect to the surface of Layer 1. (Dobrin, 1960)

The method applies to the case of several layers as well as the two layer geometry shown in the figure. One important restriction is that each successive underlying layer must have a higher velocity than the layer immediately above it.

B. ESTIMATE OF MINIMUM DEPTH TO ICE-BONDED PERMAFROST

The depth of penetration of seismic refraction energy that is recorded as a first arrival can be estimated. Such an estimate is based upon the geometry shown in Figure A-2. In the figure it is assumed that no fast layers are "seen" by the receiver array. However, it is assumed that at a point just to the right of the last geophone the first arrival energy does travel through the fast layer as shown. This is the limiting case for estimation of penetration, because if the last geophone string were longer the fast layer would be "seen".

The minimum depth estimate neglects the thin surface layer and uses known values for ν_1 and x while assuming 2400 m sec^{-1} for ν_2. Note that this velocity is slower than any velocity of ice-bonded permafrost measured during this study. The effect of the assumed ν_2 is that the calculated depth, z, is a minimum value. A representative value of ν_1 is taken as 1700 m sec^{-1}, based on the results in Table 1, so that, from Snells Law, $\beta_c = \sin^{-1}(1700/2400) = 45°$. The travel time from the shot point to the last geophone through the upper layer is

$$\Delta t_1 = \frac{x}{\nu_1}$$

while through the lower layer it is

$$\Delta t_2 = \frac{2z}{\nu_1 \cos \beta_c} + \frac{1}{\nu_2} \; (x - 2z \tan \beta_c)$$

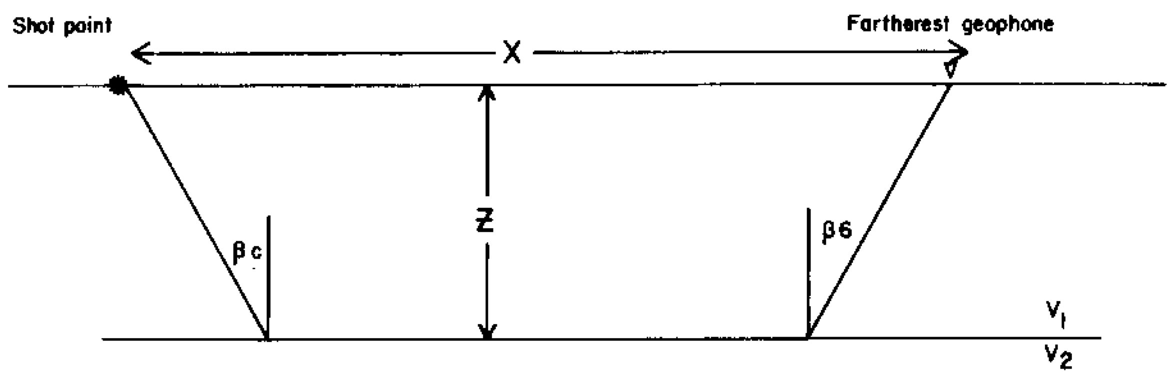

Figure A-2. Geometry of refraction signal path. The path shown is the route of the first arrival energy to a point just beyond the farthest geophone. It is assumed that the first arrival at the farthest geophone is through the top layer.

Equating these and solving for z in terms of x then gives

$$z = .22x.$$

Thus, for a separation of 200 meters between the shot and the last geophone, the minimum distance to a 2400 m sec^{-1} layer is 44m.

The method is also applicable to the multi-layer case of water and overlying non-frozen bottom. In this case a similar calculation can be made to estimate the minimum depth beneath the ocean bottom to a frozen layer that is not "seen" by the refraction equipment.

C. REDUCTION OF SEISMIC DATA

Figure A-3 shows a data plot for a short line near Point Barrow which is identified as lines 11-3 and 11-8. The approximate geographical location is region "A" of Figure 4. The time-distance curve of Figure A-3 is made in the manner shown in Figure A-1 except that the line was also reversed. Reversing is simply reshooting the line with the same geophone configuration but moving the shot point to its mirror image location at the other end of the line. Thus, 11-8 is a reversal of line 11-3. The technique is used for the detection of a sloping interface between layers 1 and 2 of Figure A-1. If the layers were homogeneous and parallel, the reversal line would be the mirror image of the original line with the reflection point being midway along the distance axis. Any variation from the ideal is generally due to a varying thickness of layer 1 or locally varying velocities in layers 1 and 2. If the layer interface were sloping the curves would not be mirror images. For this case the slope of the interface can be determined as well as the actual velocity in layer 2. Figure A-4 shows a profile of a sloping interface and a time-distance plot corresponding to that geometry.

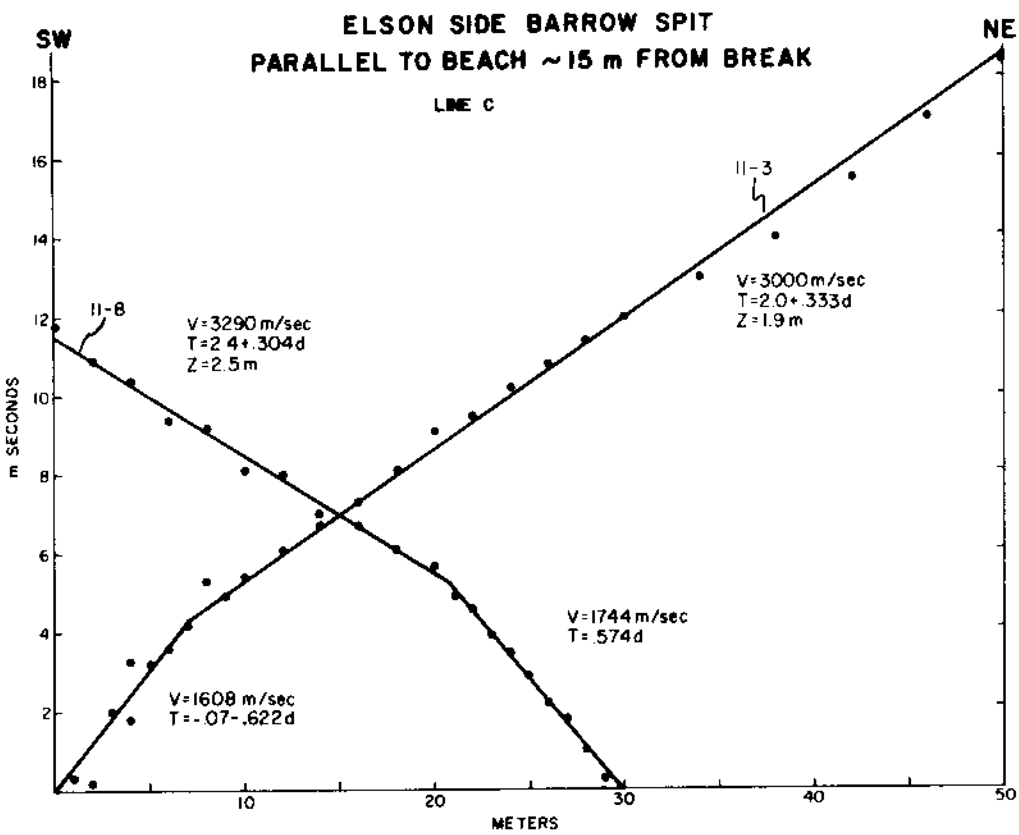

Figure A-3. Time-distance plot over a 50 meter interval along Barrow spit. Line 11-8 is a reversal of 11-3.

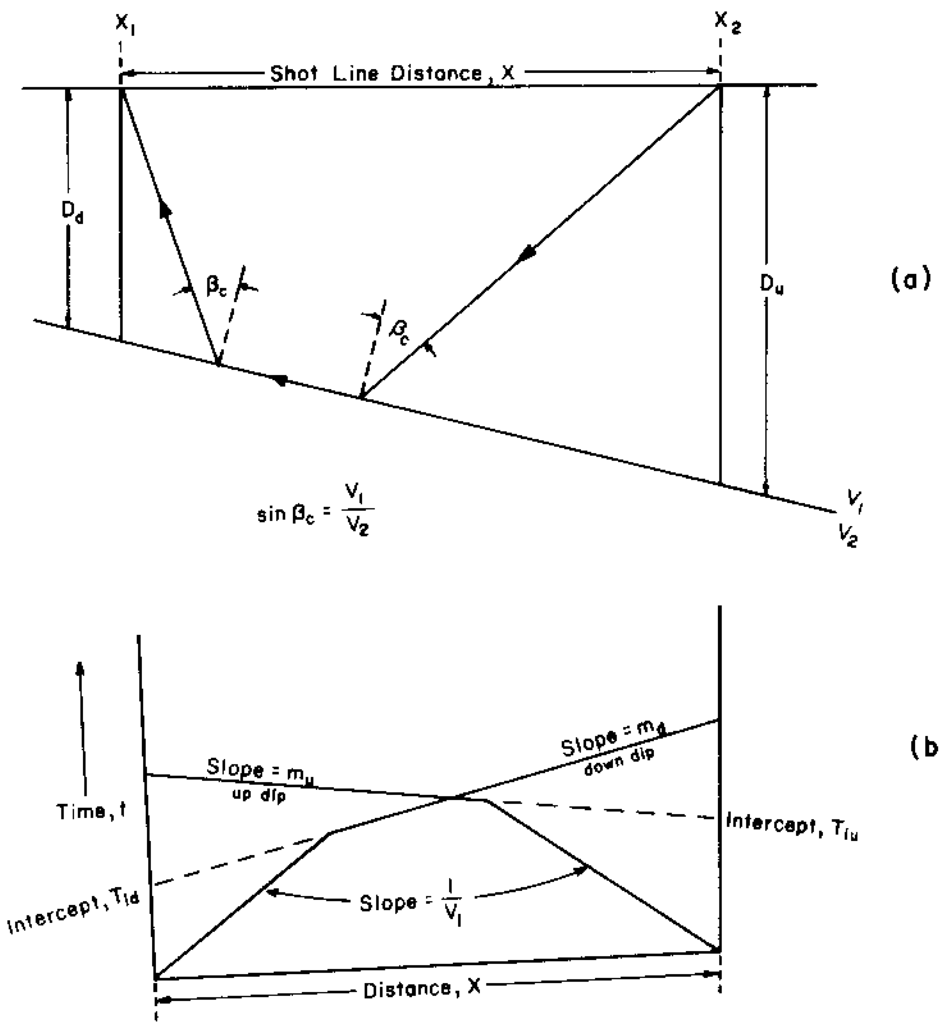

Figure A-4. Seismic wave refraction along an interface dipping at the angle α. (a) The geometry of the energy path. (b) A time distance plot for the geometry of part (a). The down dip line corresponds to a short point at X_1 with geophone placed along the shot line toward point X_2 while the up dip line corresponds to a shot point at X_2 with geophones placed toward X_1.

Several equations pertaining to Figure A-4 are given below. They relate the time-distance data plot (b) to the geometry of the sloping interface (a) (Dobrin, 1960).

$\nu_1 = \frac{1}{\text{slope}}$, for both the initial parts of the forward and reverse shots.

m_d = slope of high velocity portion of down dip data curve.

m_u = slope of high velocity portion of up dip data curve.

$$\beta_c \text{ (critical angle)} = \frac{\sin^{-1}\nu_1 m_d + \sin^{-1}\nu_2 m_u}{2}$$

$$\nu_2 = \frac{\nu_1}{\sin\beta_c}$$

$$\alpha = \frac{\sin^{-1}\nu_1 m_d - \sin^{-1}\nu_2 m_u}{2}$$

The distances from the surface to the layer interface are given by:

$$D_u = \frac{\nu_1 T_{iu}}{2\cos\beta_c\cos\alpha}, \text{ distance to interface.}$$

$$D_d = \frac{\nu_1 T_{id}}{2\cos\beta_c\cos\alpha}, \text{ distance to interface.}$$

For a non-sloping interface $\alpha = 0$ and the forward and reversed data plots become identical thus making the distance from both ends of the line to the interface the same. That is, $D_u = D_d$. Thus, the above equation can be used for any homogeneous two-layer case.

Curves 11-3 and 11-8 of Figure A-3 both have two distinct linear slopes, which correspond to P wave velocities in layer 1 and layer 2. The velocities measured in the upper layer are 1610 m sec^{-1} and 1740 m sec^{-1}, while the velocities in layer 2 are 3290 m sec^{-1} and 3000 m sec^{-1}.

The observed differences in layer 1 are attributed to measurement uncertainties and local inhomogeneities. These factors also affect the observed velocity differences in layer 2 with the added factor that the interface may be sloping. If we use the equations given above, we can determine the sloping interface angle and the distance from the shot points to the interface, D_u and D_d. The data plotted in Figure A-3 give a layer thickness of 1.9 m and 2.5 m at the ends of the shot line. Thus, it is seen that over the 30 meter length of the shot line the slope of layer 2 is small (about 0.6 m in 30 m or 2%).

In all of the data analyses we used the simple two-layer geometry because the time distance plots were found in almost all cases to be well approximated by straight lines. The exceptional case (Line A, Figure 6, Numbers 10-1, 11-1, 11-2, 12-5 and 12-6) was believed to be the result of a massive ice inclusion beneath the seismic line.

APPENDIX II

Seismic refraction data plots. The letter designators apply to Figure 6 (page 14) and Table I (page 17) while the number designators apply only to Table I.

CONTENTS

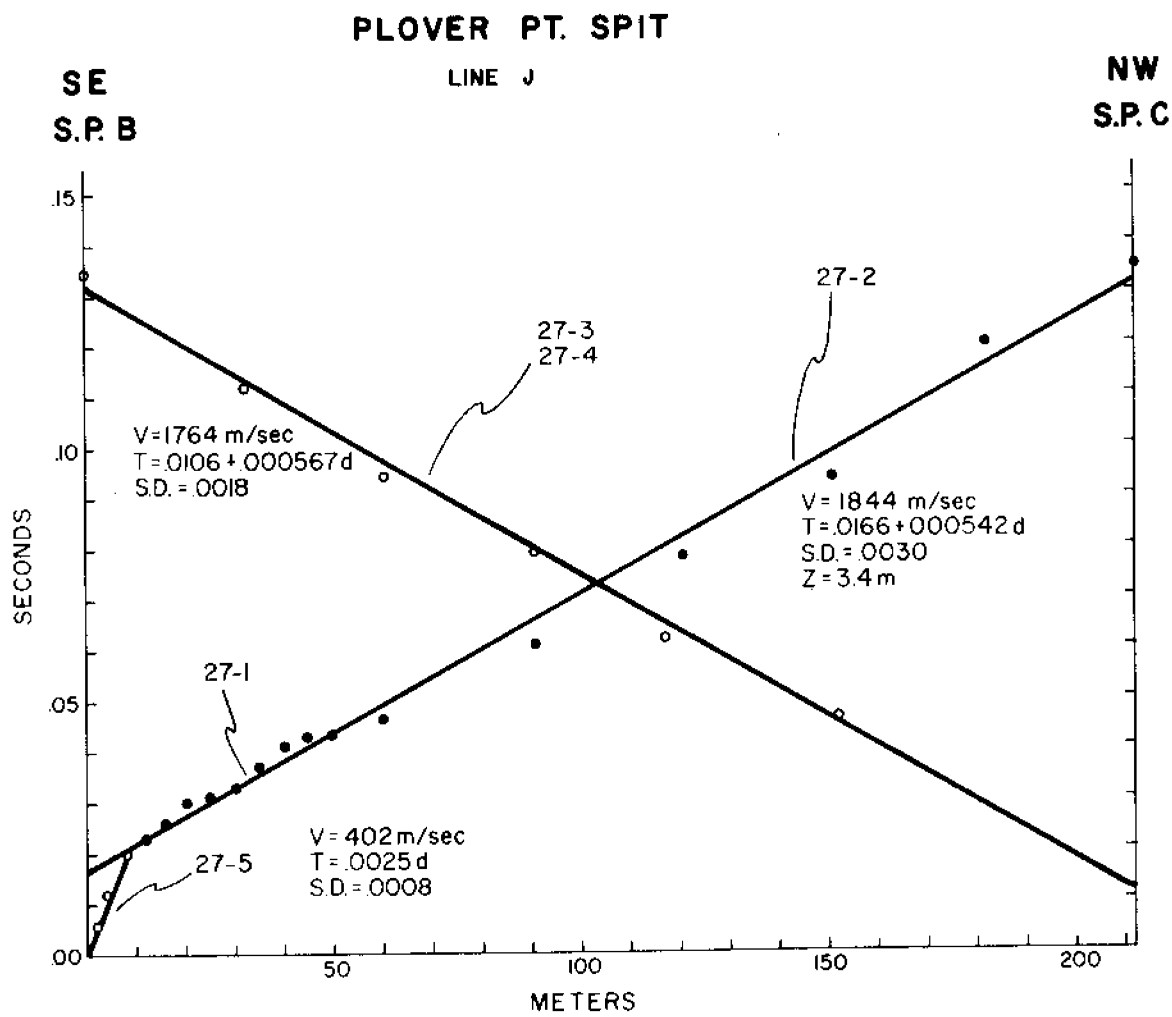

Figure A-5. Composite reversed profile on Plover Point spit.

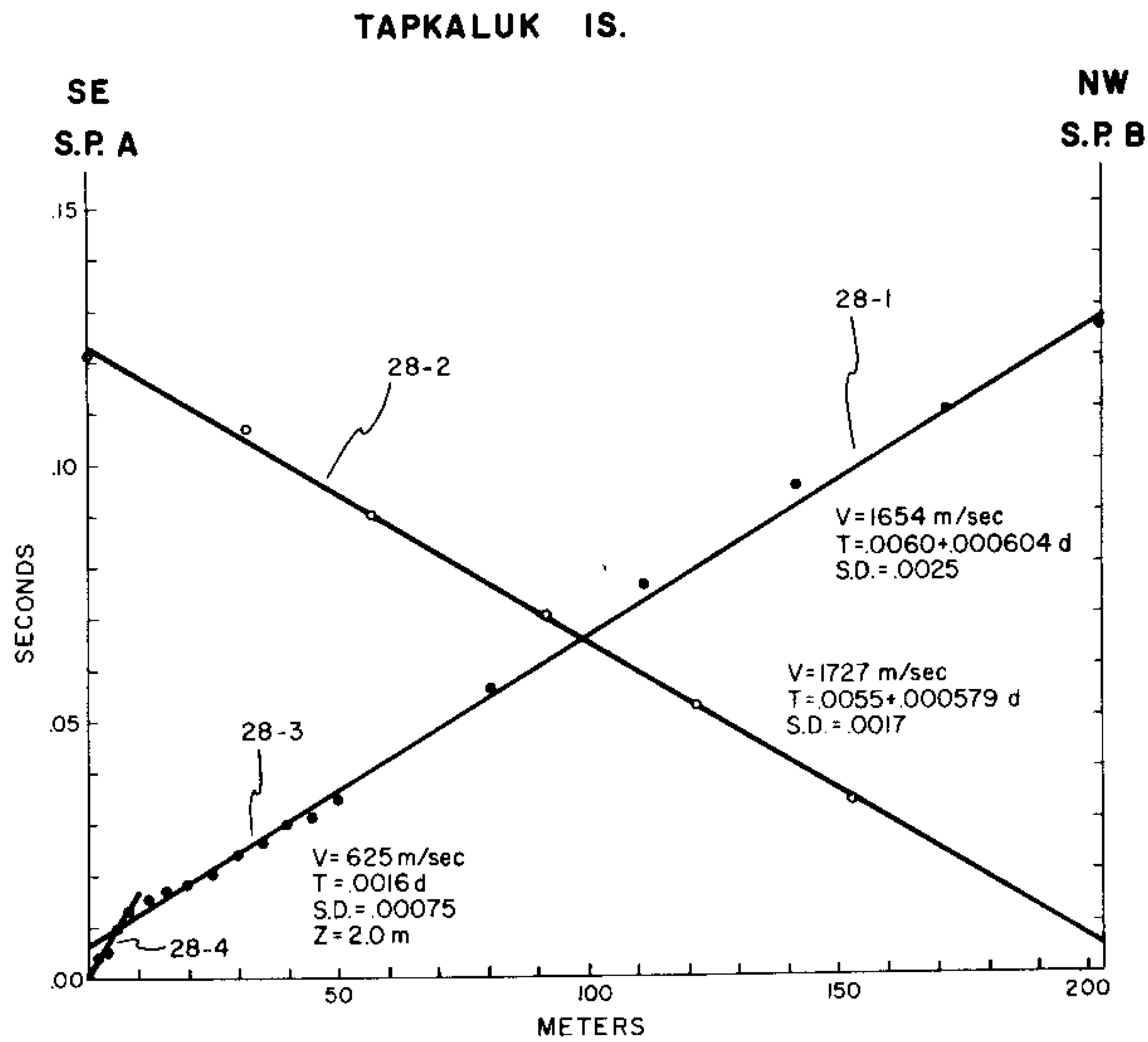

Figure A-6. Composite reversed profile in the Tapkaluk Islands.

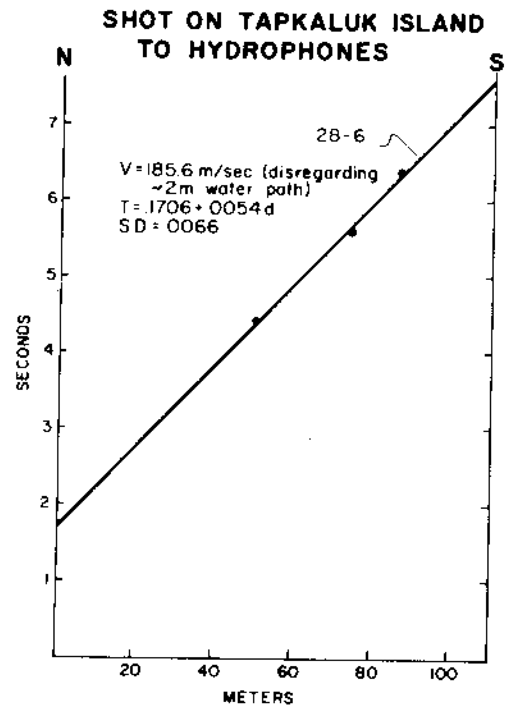

Figure A-7. Shot from Tapkaluk Islands to hydrophones in Beaufort Sea.

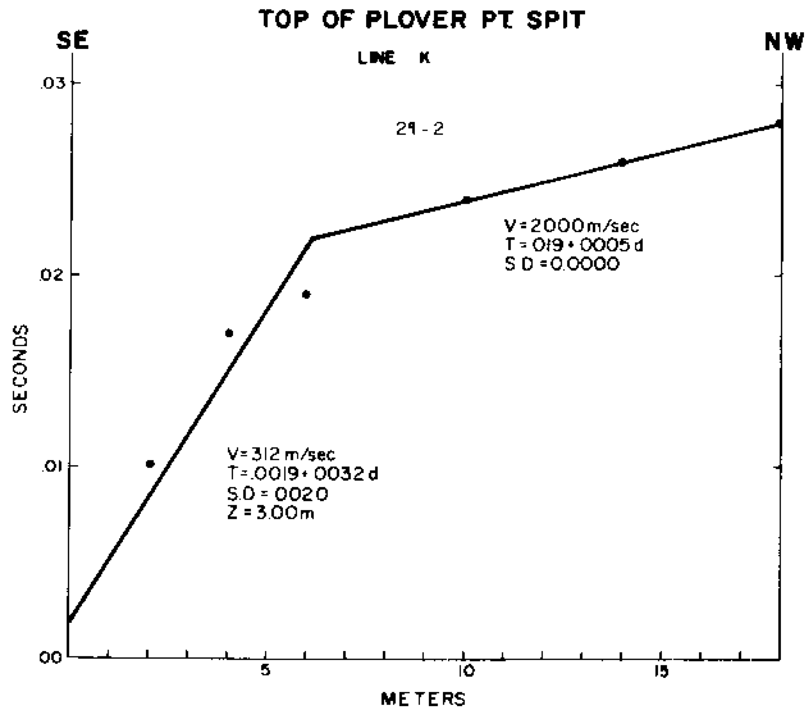

Figure A-8. Closely spaced unreversed profile on top of Plover Point spit.

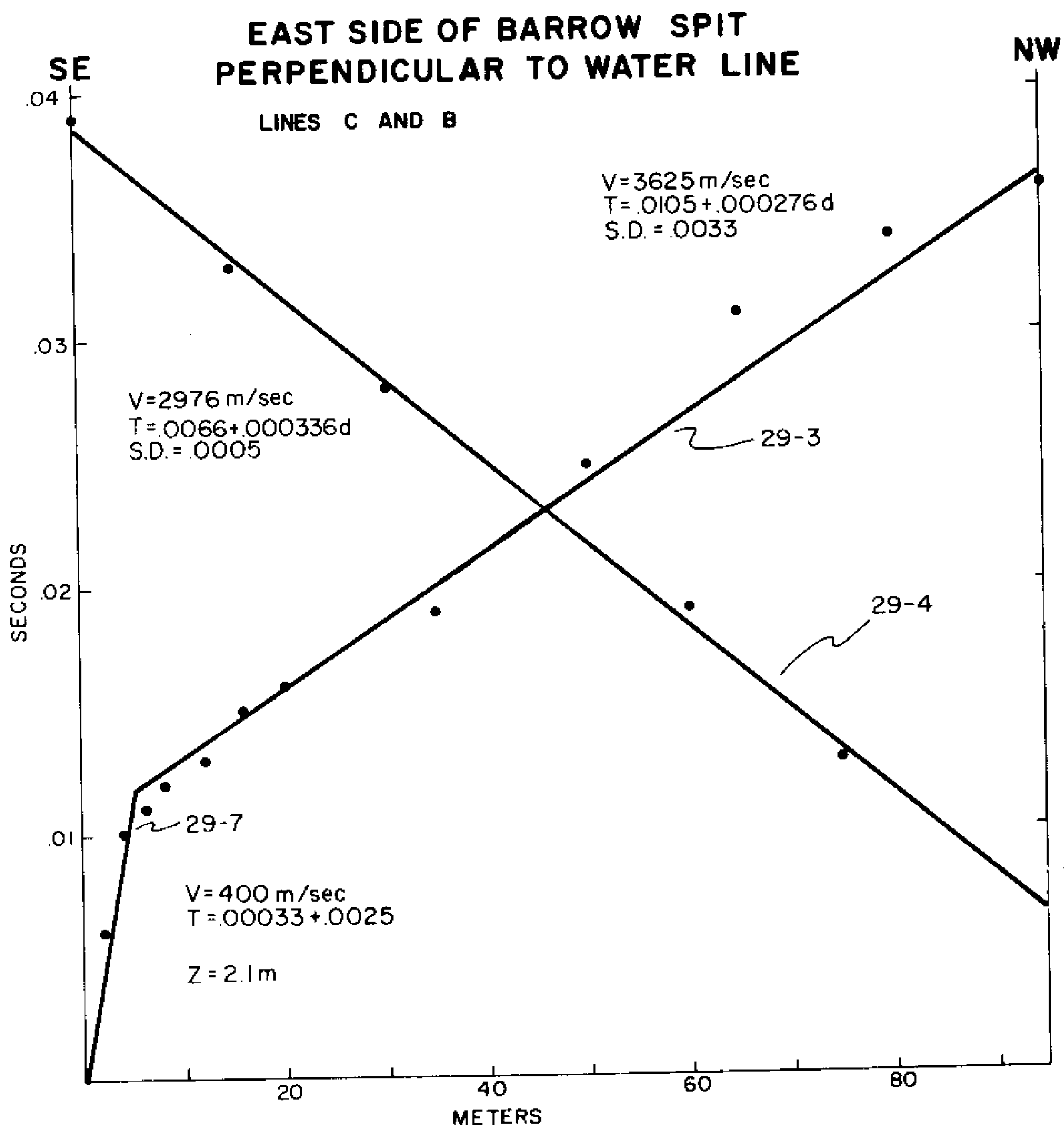

Figure A-9. Composite reversed profile perpendicular to beach on southeast side of Barrow spit.

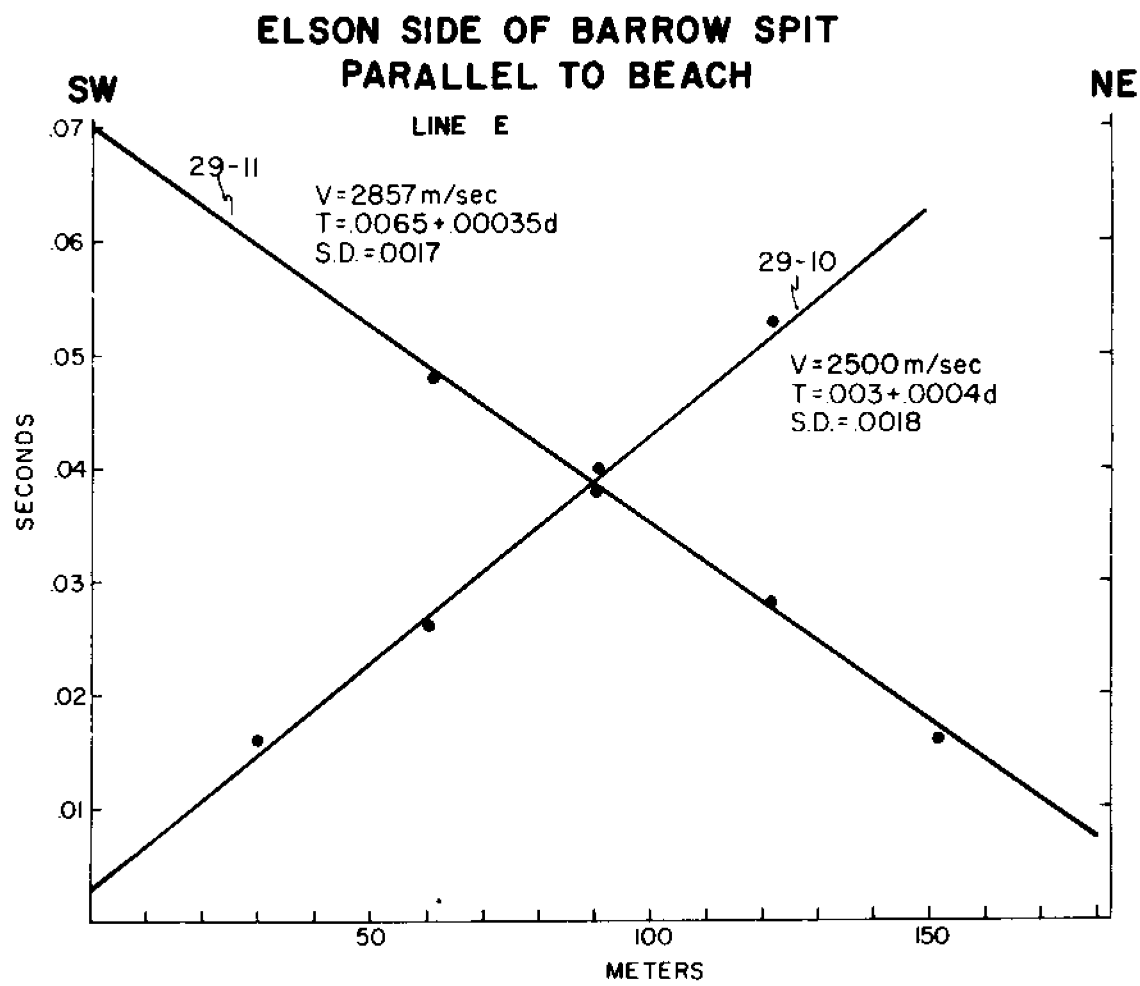

Figure A-10. Reversed profile parallel to beach on southeast side of Barrow spit.

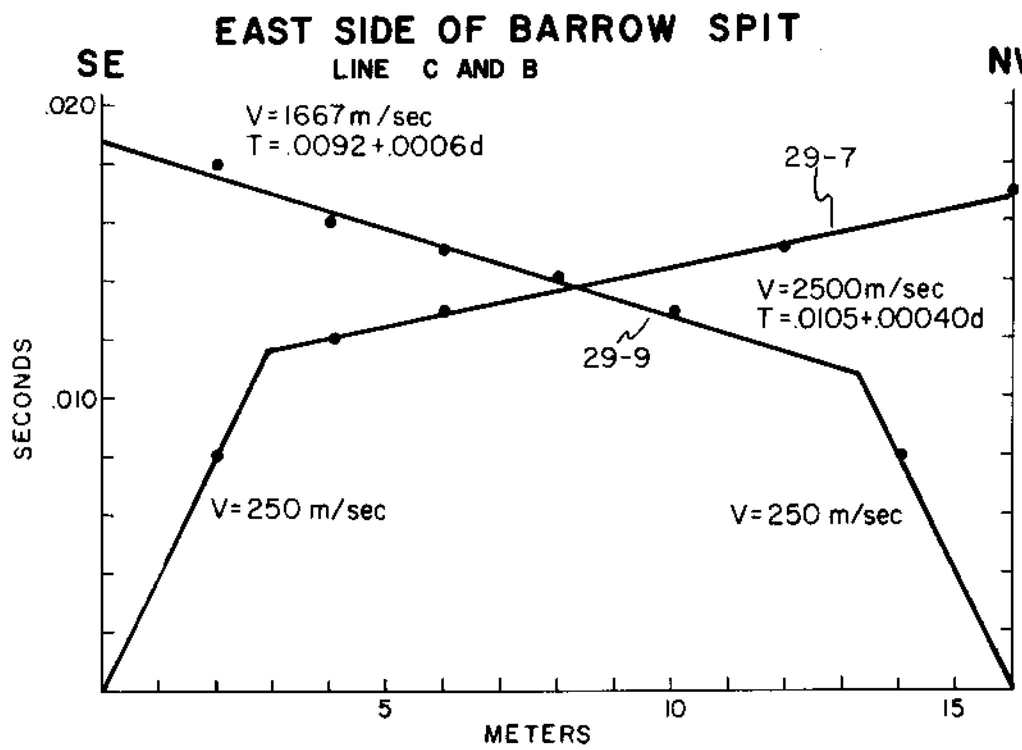

Figure A-11. Closely spaced reversed profile on southeast side of Barrow spit.

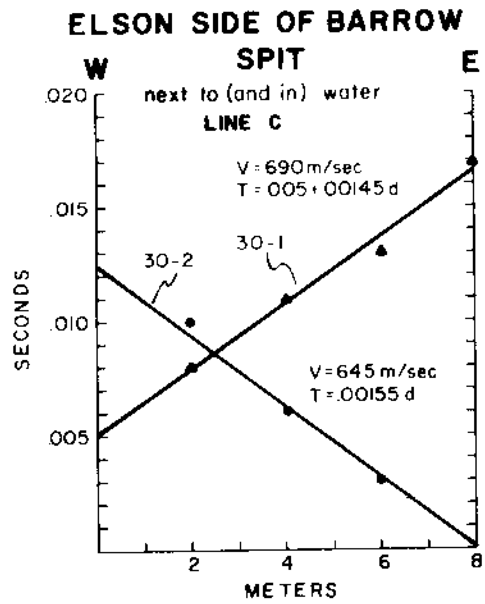

Figure A-12. Closely spaced reversed profile partly in water on southeast side of Barrow spit.

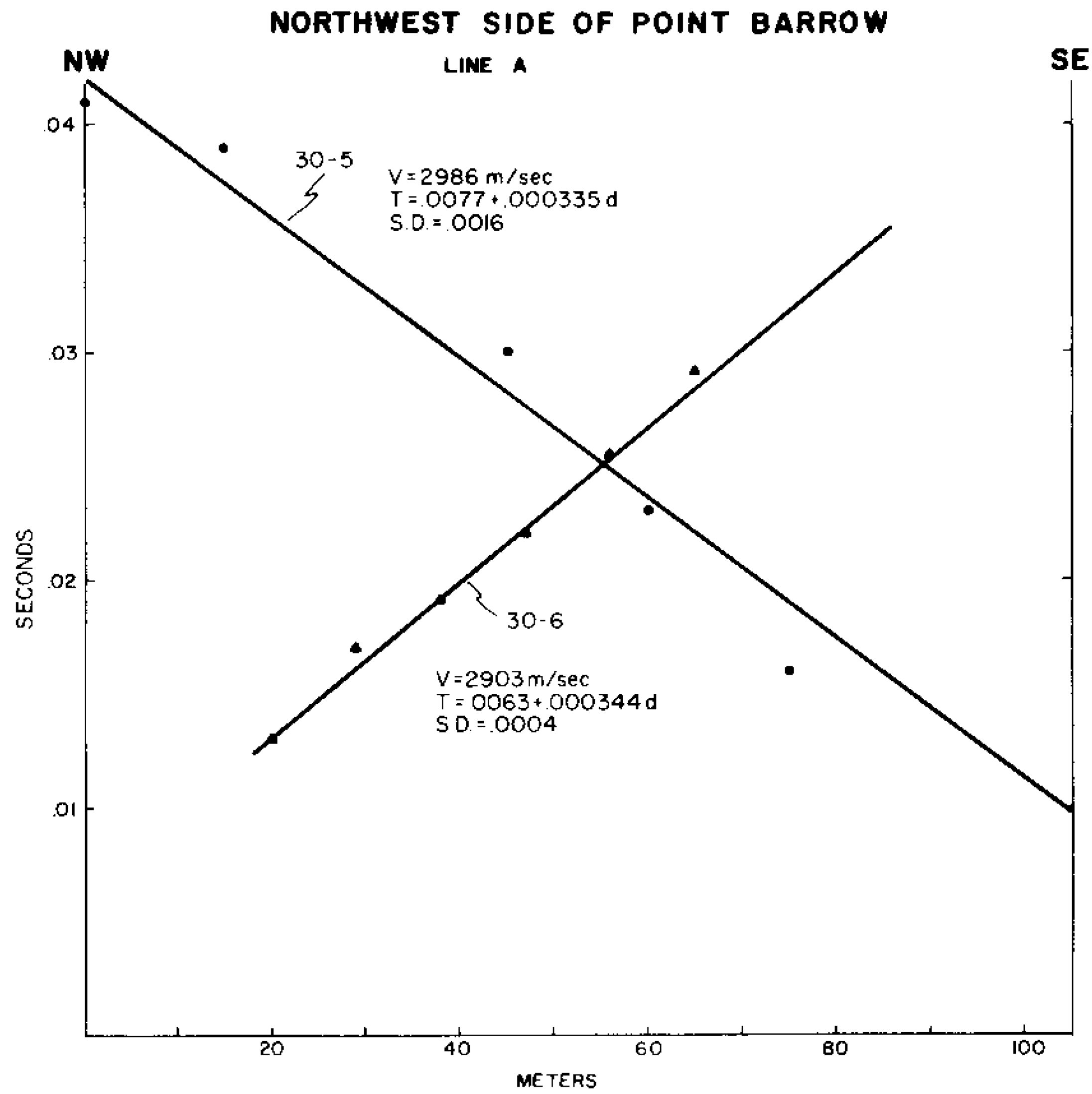

Figure A-13. Reversed profile on northwest side of Barrow spit.

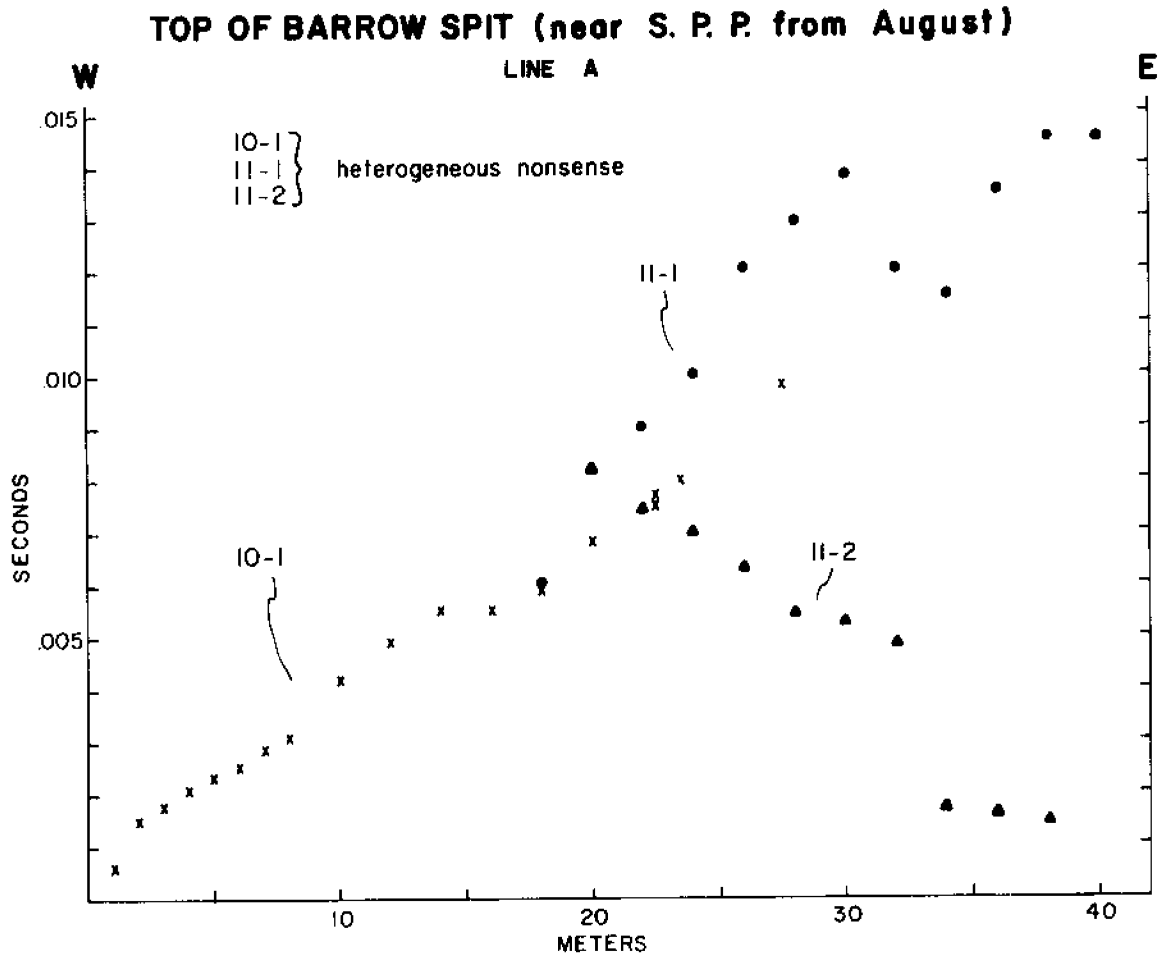

Figure A-14. Top of Barrow spit and Chukchi Sea side of Pt. Barrow. Velocities and arrival times very anomalous.

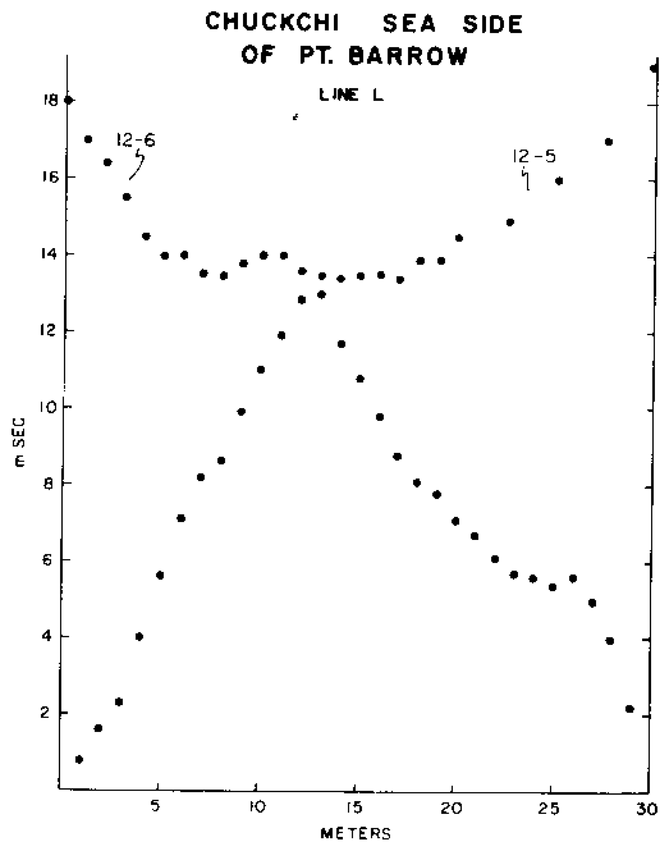

Figure A-15. Top of Barrow spit and Chukchi Sea side of Pt. Barrow. Velocities and arrival times very anomalous.

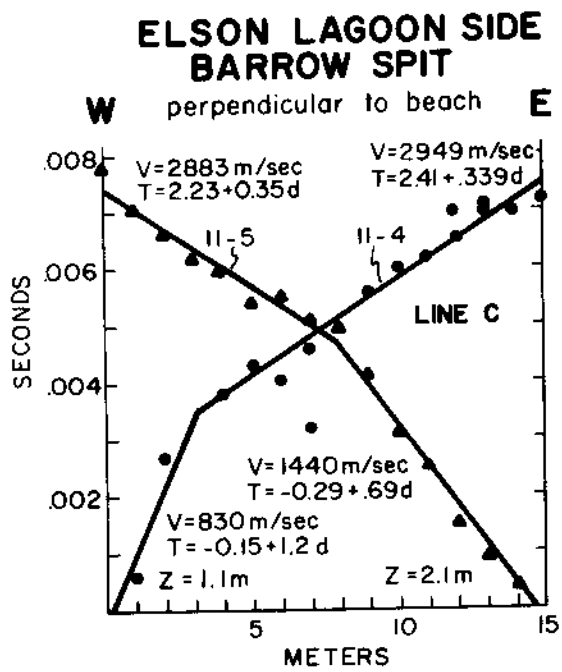

Figure A-16. Reversed profile near concave side of Barrow spit perpendicular to beach near C.

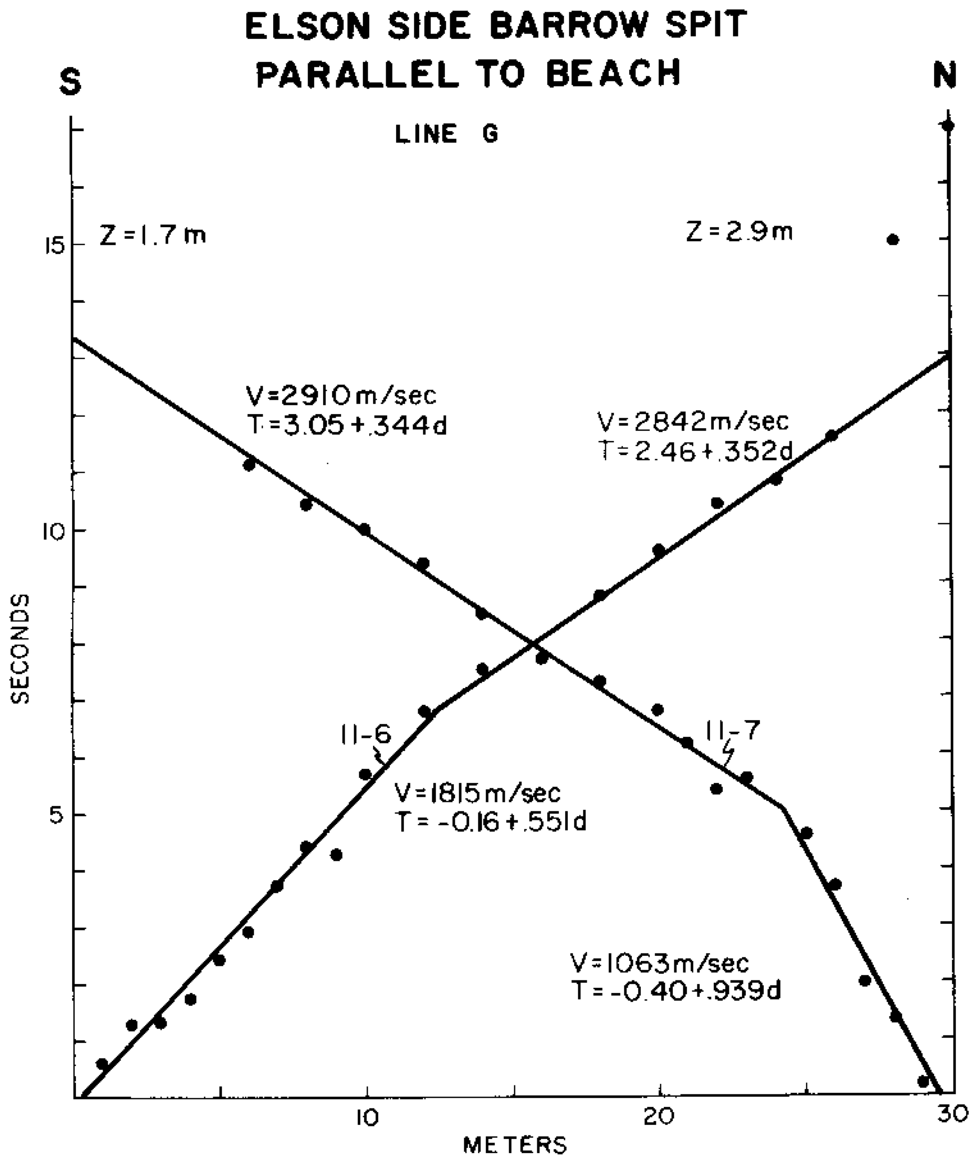

Figure A-17. Reversed profile on southeast side of Barrow spit parallel to beach (approx. 12 m to beach).

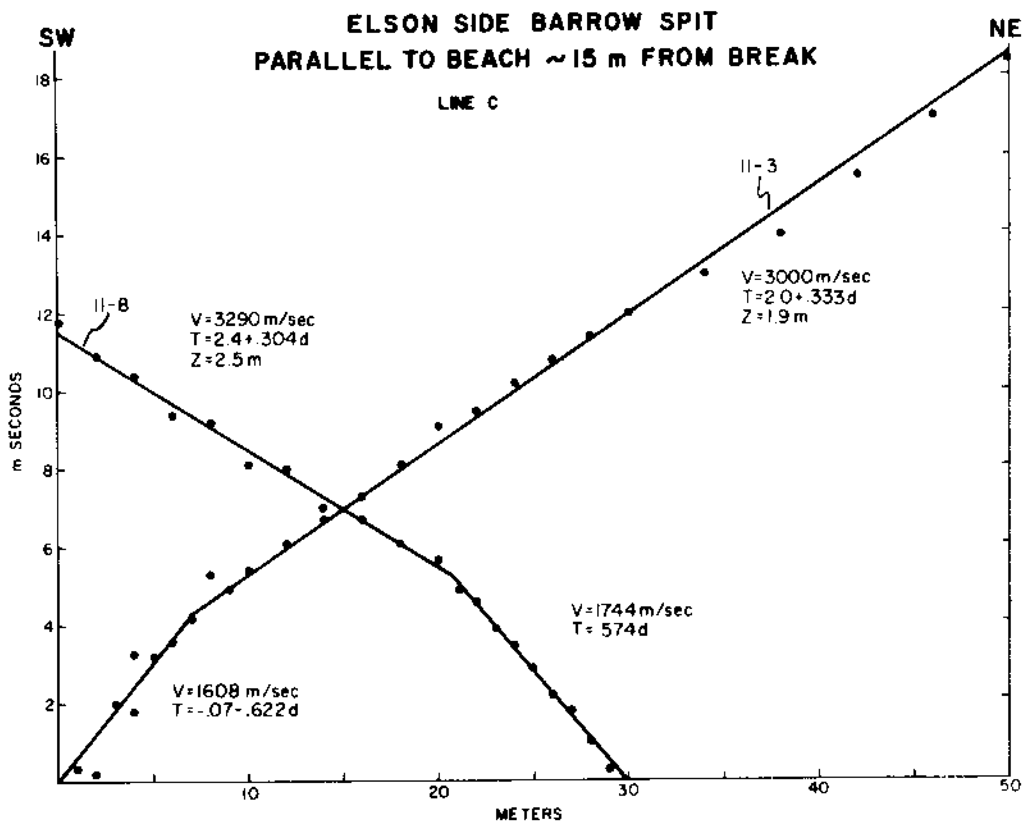

Figure A-18. Profiles near concave side of Barrow spit.

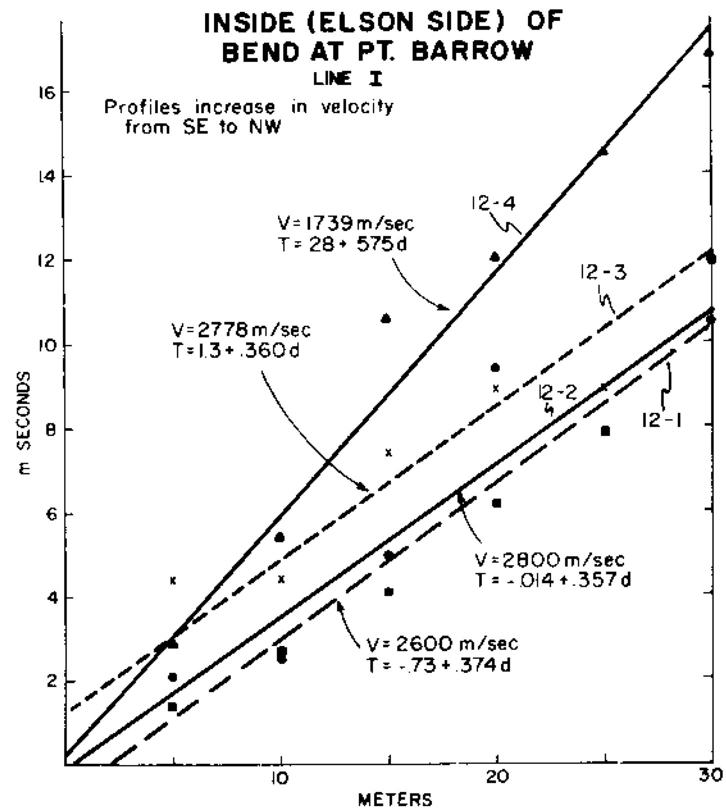

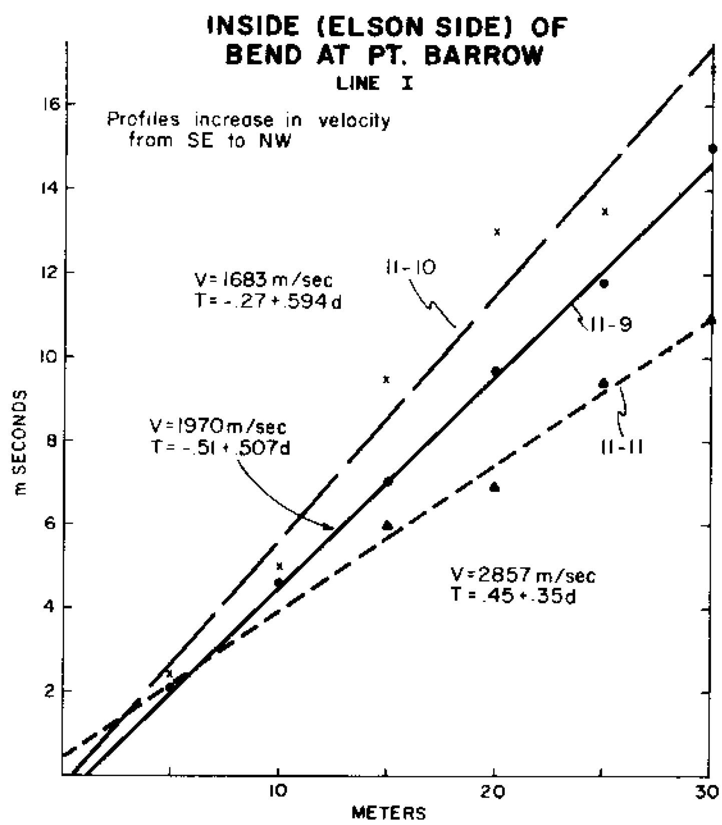

Figure A-19. Profiles near concave side of Barrow spit.

BARROW- MEAT CELLAR

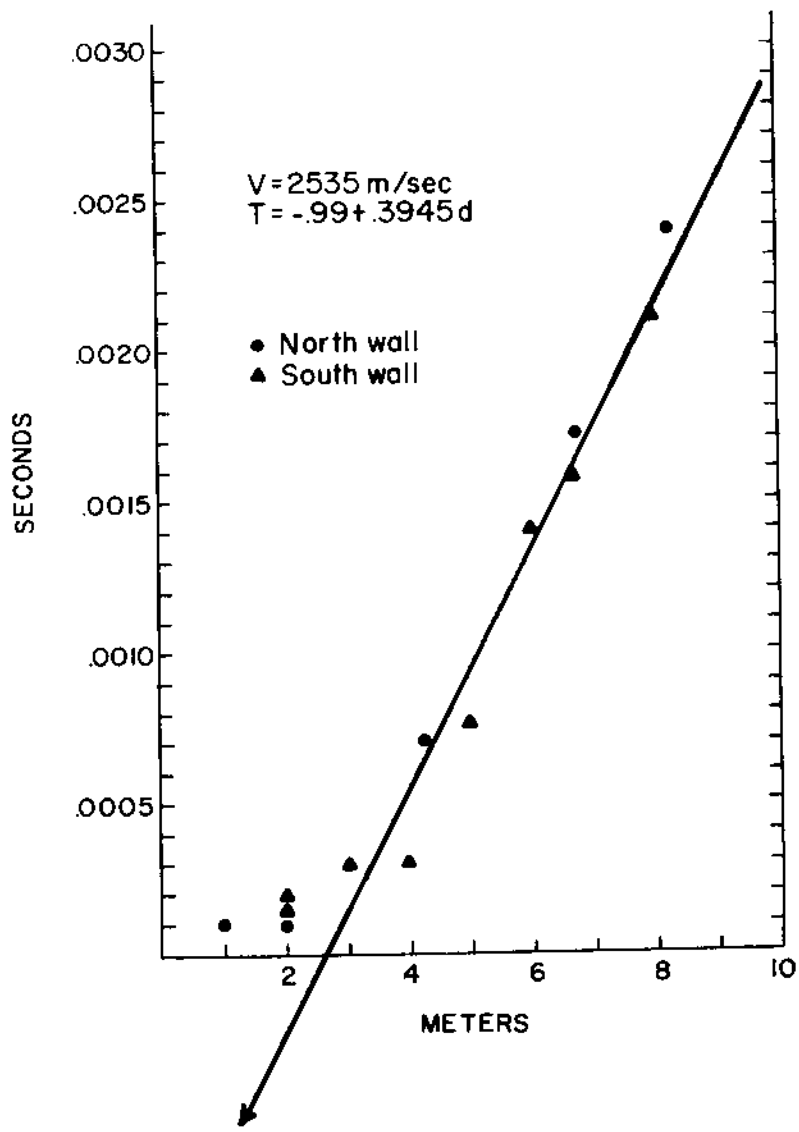

APPENDIX III

THERMISTOR CALIBRATION DATA

Ice point data for the 50-meter Aanderaa thermistor cable are summarized here. Temperatures are determined from the characteristics of Fenwal GB 32JM19 thermistors corrected with these data. Calibration was done using a modified Leeds and Northrup 4289 Wheatstone Bridge at a current of about 20 micro-amps. Standard error is about 1 ohm or slightly less. The identification of the pins in the cable termination plug is as follows:

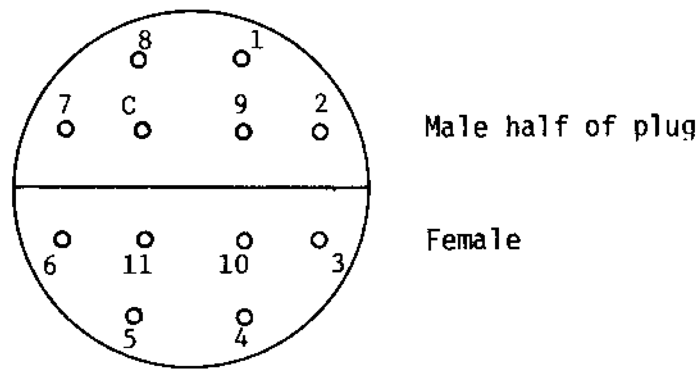

Thermistor #1 is nearest the plug, and "c" is the common lead.

Thermistor Number	Resistance
1	5.7040 10^3 ohm
2	5.6930 "
3	5.6964 "
4	5.5951 "
5	5.7120 "
6	5.6960 "
7	5.7054 "
8	5.7240 "
9	5.7005 "
10	5.7019 "
11	5.7068 "

Additional information can be obtained from Aanderaa at:

Hardangervein 2
5050 Nesttun
Norway

APPENDIX IV

THAWING OF OCEAN-INUNDATED FROZEN GROUND FROM THE WATER INTERFACE

The model is illustrated by the following sketch:

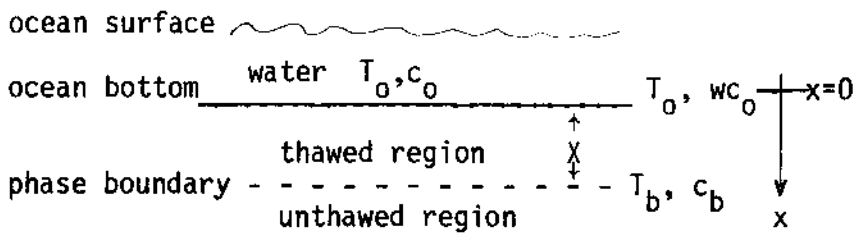

The following notation applies:

x = vertical coordinate, positive down

t = time

T = temperature

w = volume fraction of water in thawed region

c = salt concentration per unit bulk volume

X = thickness of thawed region

κ_t = thermal diffusivity of thawed region

K = thermal conductivity of thawed region

κ_s = bulk diffusivity of salt in thawed region

h = volumetric latent heat

T_f = freezing temperature of sea water

T_o = ocean bottom temperature

T_b = temperature at phase boundary (bottom of thawed region)

c_o = salt concentration in sea water

c_b = salt concentration at phase boundary

The equations describing the model are:

$$\kappa_t \frac{\partial^2 T}{\partial x^2} = \frac{\partial T}{\partial t}$$

$$\kappa_s \frac{\partial^2 c}{\partial x^2} = \frac{\partial c}{\partial t}$$

Since we are neglecting heat capacity, the initial temperature can be taken to be T_o. Initially $X = 0$. At the ocean bottom ($x = 0$) we have $T = T_o$, and at the lower boundary ($x = X$) we have

$$\frac{dX}{dt} = - \frac{K}{h} \frac{\partial T}{\partial x} \bigg|_b$$

$$\frac{dX}{dt} = -\kappa_s \frac{1}{c_b} \frac{\partial c}{\partial x} \bigg|_b$$

$$c_b = w \; c_o \frac{T_b}{T_f}$$

The subscript b implies evaluation at the lower boundary. The last relation assumes that the freezing point of sea water varies linearly with salt concentration, which is an approximation.

It is consistent with the neglect of heat capacity to assume that the temperature varies linearly with x. This is a good approximation, and although one can find a solution in closed form without it, it does simplify the calculations considerably. Then,

$$T = T_o + \frac{(T_b - T_o)}{X} \; x$$

satisfies the boundary conditions. The differential equation for c and the condition at the upper boundary (sea water concentration) are satisfied by

$$c = wc_o\left(1 - A \operatorname{erf} \frac{x}{\sqrt{4\kappa_s t}}\right)$$

where $\operatorname{erf} u = \frac{2}{\sqrt{\pi}} \int_0^u e^{-\nu^2} d\nu$, and A is a constant to be determined from the conditions at the lower boundary. It is straightforward to show that all these conditions are satisfied if

$$X = (p \sqrt{4\kappa_s}) \sqrt{t},$$

where the constant p is determined from the transcendental equation

$$\sqrt{\pi}\, p\, e^{p^2} \operatorname{erf} p = \frac{1}{\frac{T_o}{T_f} + 2\left(\frac{\kappa_s h}{-kT_f}\right)p^2} - 1,$$

and

$$A = \left\{\frac{T_o}{T_f} + 2\left(\frac{\kappa_s h}{-kT_f}\right) p^2\right\} \sqrt{\pi}\, p\, e^{p^2}.$$

If κ_s is small enough

$$\sqrt{\pi}\, p\, e^{p^2} \operatorname{erf} p \approx \frac{T_f}{T_o} - 1$$

and

$$A \approx \left(\frac{T_o}{T_f}\right) \sqrt{\pi}\, p\, e^{p^2}.$$